Mineralogy and Genesis of the Polymetallic and Polyphased Low Grade Fe-Mn-Cu Ore of Jbel Rhals Deposit (Eastern High Atlas, Morocco)

Verhaert, Michèle; Bernard, Alain; Saddiqi, Omar; Dekoninck, Augustin; Essalhi, Mourad; Yans, Johan

Published in:
Minerals

DOI:
10.3390/min8020039

Publication date:
2018

Document Version
Publisher's PDF, also known as Version of record

minerals

MDPI

Article

Mineralogy and Genesis of the Polymetallic and Polyphased Low Grade Fe-Mn-Cu Ore of Jbel Rhals Deposit (Eastern High Atlas, Morocco)

Michèle Verhaert [1,*], Alain Bernard [2], Omar Saddiqi [3], Augustin Dekoninck [1], Mourad Essalhi [4] and Johan Yans [1]

1 Department of Geology, Institute of Life-Earth-Environment (ILEE), Université of Namur, Rue de Bruxelles 61, 5000 Namur, Belgium; augustin.dekoninck@unamur.be (A.D.); johan.yans@unamur.be (J.Y.)
2 Département des Sciences de la Terre et de l'Environnement, Laboratoire de Minéralogie et Géochimie Appliquée, Université Libre de Bruxelles, Avenue F.D. Roosevelt 50, 1050 Brussels, Belgium; abernard@ulb.ac.be
3 Laboratoire Géosciences, Université Hassan II, BP 5366, Maârif, 20100 Casablanca, Morocco; omarsaddiqi@yahoo.fr
4 Equipe de Recherche: Géophysique, Géoresources et Patrimoine, Faculté des Sciences et Techniques, Université Moulay Ismaïl, BP. 509, Boutalamine, 52000 Errachidia, Morocco; mourad.essalhi@gmail.com
* Correspondence: michele-alexandra.verhaert@unamur.be; Tel.: +32-81-724-474

Received: 13 December 2017; Accepted: 19 January 2018; Published: 25 January 2018

Abstract: The Jbel Rhals deposit, located in the Oriental High Atlas of Morocco, hosts a polymetallic Fe-Mn-Cu ore. Large metric veins of goethite and pyrolusite cut through Paleozoic schists that are overlaid by Permian-Triassic basalts and Triassic conglomerates. The genesis of this deposit is clearly polyphased, resulting from supergene processes superimposed over hydrothermal phases. The flow of Permian-Triassic basalts probably generated the circulation of hydrothermal fluids through the sedimentary series, the alteration of basalts and schists, and the formation of hydrothermal primary ore composed of carbonates (siderite) and Cu-Fe sulfides. Several episodes of uplift triggered the exhumation of ores and host rocks, generating their weathering and the precipitation of a supergene ore assemblage (goethite, pyrolusite, malachite and calcite). In the Paleozoic basement, Fe-Mn oxihydroxides are mostly observed as rhombohedral crystals that correspond to the pseudomorphose of a primary mineral thought to be siderite; goethite precipitated first, rapidly followed by pyrolusite and other Mn oxides. Malachite formed later, with calcite, in fine millimetric veins cutting through host-rock schists, conglomerates and Fe-Mn ores.

Keywords: Moroccan High Atlas; supergene deposits; goethite; gossan; weathering

1. Introduction

The Jbel Rhals Fe-Mn-Cu deposit is located in the Moroccan Oriental High Atlas, 20 km south from Bou Arfa city (Figure 1). Several ore deposits in the Bou Arfa district were mined in the first half of the 20th century, and are recently (re)considered in several papers: Jbel Klakh (Cu) [1,2], Jbel Haouanit (Pb-Zn-Cu-V) [1,2], Hamarouet and Aïn Beida (Mn) [3]. The Jbel Rhals locality was known as a Cu deposit for centuries and has been shortly exploited during the 19th–20th centuries; some mining activities started up again in 2012.

However, there is no mineralogical inventory of the Jbel Rhals deposit, and processes leading to the formation of the various mineral phases have not been investigated yet. The issue of the origin and genesis of these ores has not been raised either. This work presents a petrological, mineralogical, and geochemical synthesis of the Jbel Rhals deposit. We focus our investigation mainly

on the supergene processes responsible for the current ore mineralogy, considering that the primary mineralization is not exposed in outcrops or pits, nor in galleries, and that only the oxidation zone of the deposit is accessible. The purpose of this study is to investigate and highlight relationships between mineral associations and host rocks, to identify parageneses, and to propose a metallogenic model in order to explain the genesis of the ores. Special attention is also paid to the potential concentration of some elements classified as "strategic" or "critical" raw materials by the European Union (Light Rare Earth Elements (LREE), Heavy Rare Earth Elements (HREE), Y, In) in supergene mineral phases.

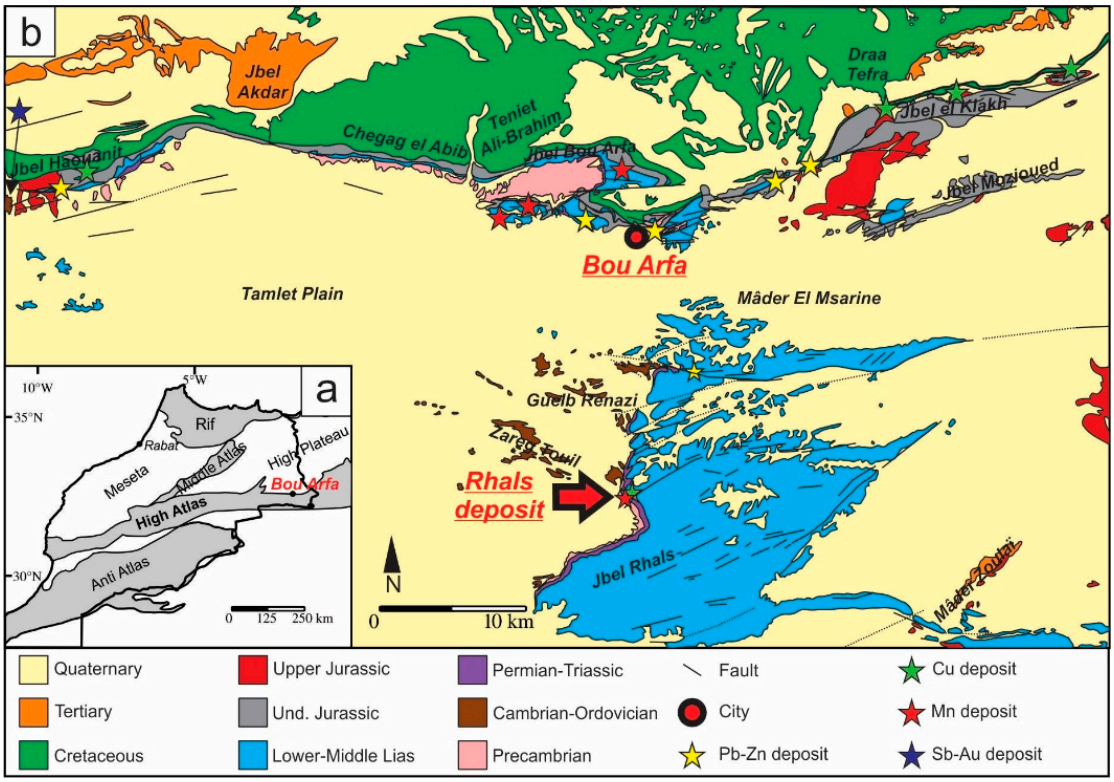

Figure 1. (**a**) Simplified geologic map of parts of Morocco and location of Bou Arfa; (**b**) Synthetic geologic map of the Bou Arfa region generalized according to the ages of units and showing the location of the Jbel Rhals ore deposit (modified from [4]).

Geological Setting

The Jbel Rhals deposit is located at the northern edge of the Oriental High Atlas (Figure 1). This intracontinental mountain belt extends WSW to ENE, from the Atlantic coast to Algeria where it continues in the so-called "Saharan Atlas". The geodynamic evolution of the High Atlas system involves the interplay of two main events: (1) the Triassic to late Cretaceous pre-orogenic rifting and subsequent filling of the basins, and (2) the Cenozoic basin inversion leading to the shortening of basement and cover units, formation of syn-orogenic basins, and uplift [5–7].

The break-up of Pangaea and the opening of the Tethys and Atlantic Oceans triggered the formation of intracontinental rifts that affected the Variscan basement and induced the thinning of the North African crust [8]. The Triassic is characterized by the transition from a distensive to a transtensive context: narrow subsident basins, separated in horsts and grabens, developed during the first part of this period [8,9], while pull-apart basins were induced during the second one [10]. Rifting aborted during the late Triassic [8]. During Liassic, a sinistral transform zone induced the division of the Atlasic basin into two trenches that later became the Middle and High Atlas [8,11]. Synrift basins contain a succession of Permian to Triassic red-bed sedimentary rocks (conglomerate, sandstone, siltstone and mudstone), with widespread evaporites and intercalated basaltic and lava

flows, followed by Jurassic-Cretaceous carbonates and marls [5]. The flow of ca. 210–195 Ma basalts and dolerites is related to the Central Atlantic Magmatic Province (CAMP) [5,12–14]. Following [5,14], the geochemical signature of these rocks is typical of continental intraplate magmatism, and more precisely of continental tholeiites (flood basalts); their common slight enrichment in incompatible elements implies a potential crustal contamination during rising.

By the end of Cretaceous, the opening of Atlantic Ocean changed the drifting direction of the African plate from heading E to NE, in convergence with the Iberian (Eurasiatic) plate. In response, constraints switched from being extensional to compressional, leading to basin inversion [11,15]. Shortening occurred by fracturing and folding the Mesozoic-Cenozoic cover units and the Variscan basement, and sometimes by detachment of cover units from the basement [5,12,16]. Three major episodes of exhumation are defined in the Eastern High Atlas: late Eocene (between Lutetian and Bartonian), early to middle Miocene, and late Pliocene to Quaternary [6]. The last episode, which corresponds to the paroxysmal compression phase, is responsible for the building of the current orogeny, and contributes to most of the High Atlas topography, together with lithospheric thinning [17].

The Jbel Rhals ore deposit (32°20′40.6″ N; 1°58′40.6″ W), elevated between 1200 and 1300 m in altitude, is located at 20 km south of the city of Bou Arfa, in the Figuig province of Morocco (Figure 1). The deposit is situated in a Precambrian-Liassic inlier, at the base of a 200 m high cliff (Figure 2a), eastward of the Tamlet plain which is filled with various Quaternary materials, and south of Jurassic-Cretaceous reliefs hosting supergene Cu-Pb-Zn-V ore deposits (Figure 1) [1]. The place is also known as "Guelb en Nahas", which means the "Copper Hill" in Arabic, referring to some ancient mining activities by Portuguese miners for copper ores. The Cu mineralization has been somewhat mined during the 20th century, but received little attention since closure of the deposit until 2012, when a project of mining recovery was submitted. Ores were/are mined in shafts and subhorizontal galleries of several tens of meters long and about two meters high, driven into the Paleozoic basement rocks (Figure 2b). The shafts are not accessible anymore. The stratigraphic succession of the entire area (mapped by [4]) is complex: the intense fracturing and moderate folding of the series disrupt the sedimentary structures arrangement, and most original features are no more apparent. Several NE-SW normal faults are observable in the deposit area (Figure 1), one of which, close to the ores, triggers a pluri-decametric displacement in the Triassic-Jurassic series.

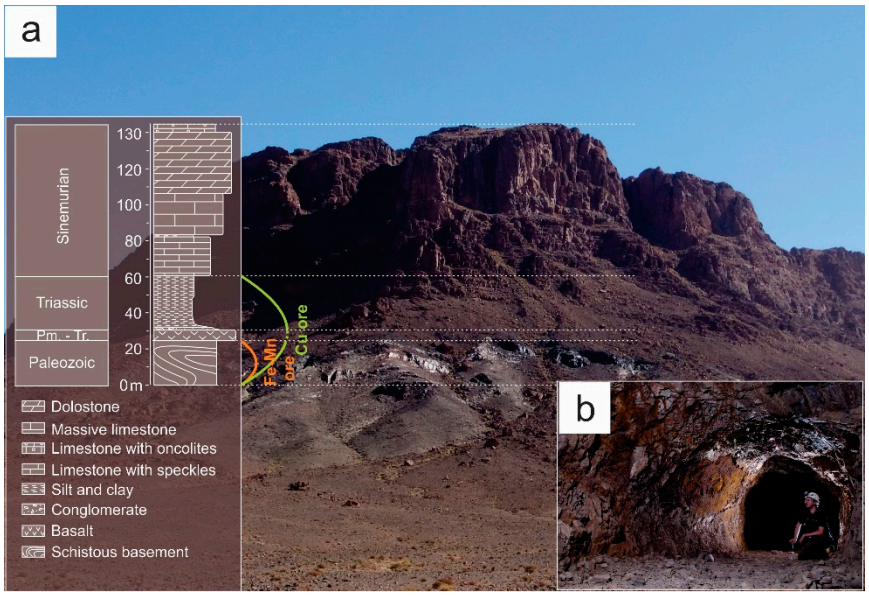

Figure 2. (**a**) Field view of Jbel Rhals and stratigraphic log of the observed units (modified after [3]); (**b**) mining gallery showing Fe-Mn mineralization.

The basement is constituted of Paleozoic shales that are successively covered by Triassic conglomerates, Triassic silty layers, and Jurassic dolomitized series (Figure 2a). Permian-Triassic basalts are found between the basement and Triassic-Jurassic series (Figure 2a). The several meters thick Fe-Mn ore is confined to the Paleozoic shales, right under the Permian-Triassic basalts (Figure 2a), while Cu-mineralized veins extend from the Paleozoic shales (and the Fe-Mn ore) to the Triassic conglomerates. The thickness of the shale beds ranges from 1 centimeter to several decimeters. Stratification is subvertical in the Paleozoic shales (Figure 3a), but horizontal in the Triassic and Sinemurian formations.

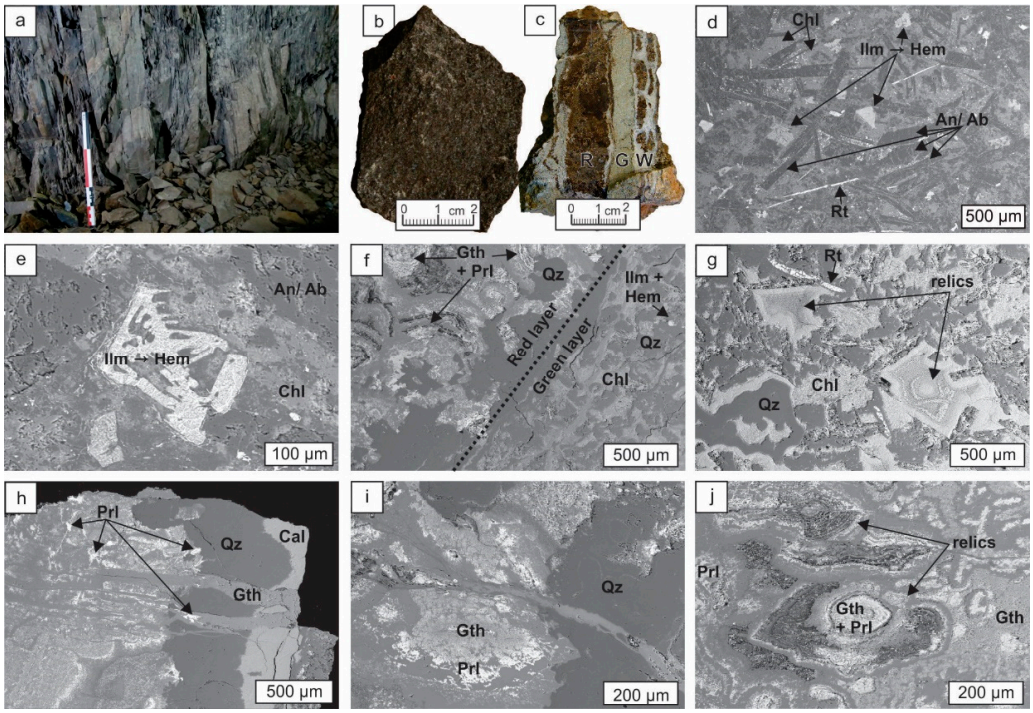

Figure 3. Host rocks (**d**–**j**: SEM (Scanning Electron Microscope) photomicrographs, in backscattered electrons mode). (**a**) Paleozoic schisteous host rock (the scale is 30 cm long); (**b**) Permian-Triassic poorly weathered basalt; (**c**) most altered/weathered basalt composed of three different layers: red (R), green (G) and white (W); (**d**) poorly weathered basalt, with albite (Ab) and anorthite (An) laths, rutile (Rt), chlorite (Chl), and ilmenite (Ilm) weathered in hematite (Hem); (**e**) skeletal ilmenite (Ilm) presenting exsolution lamellae of hematite (Hem), in the poorly weathered basalt; (**f**) transition between the red and the green altered/weathered layers of the basalt, with goethite (Gth), pyrolusite (Prl), chlorite (Chl), quartz (Qz) and ilmenite-hematite (Ilm + Hem); (**g**) quartz (Qz), chlorite (Chl), rutile (Rt) laths, and relics of primary minerals in the green part of most altered/weathered basalt; (**h**) border between red and white parts of the most altered/weathered basalt, with quartz (Qz), calcite (Cal), goethite (Gth), and pyrolusite (Prl); (**i**) transition between the red and the white layers of the most altered/weathered basalt, with quartz (Qz), goethite (Gth), pyrolusite (Prl); (**j**) goethite (Gth) and pyrolusite (Prl) forming concentric structures in relation to relics of primary minerals, in the red part of most altered/weathered basalt.

2. Materials and Methods

Thirty samples were collected in March 2014. X-Ray diffraction was carried out on twenty-one samples in order to identify the major mineral phases of the ore, using a BRUKER X-ray diffractometer (Bruker, Billerica, MA, USA) with a HI STAR GADDS (General Area Detector Diffraction System) CuKα detector. One thin section of the "freshest" basalt was observed in transmitted light mode with a LEITZ HM-POL petrographic polarizing microscope (Microscope Central, Feasterville, PA, USA). Twenty-one polished sections were observed on a ZEISS PHOTOMICROSCOPE reflection microscope

(Carl Zeiss AG, Oberkochen, Germany), and with a JEOL JXA-8600 SUPERPROBE scanning electron microscope (SEM) (JEOL, Tokyo, Japan) coupled to an energy dispersive electron spectrometer (EDS).

Geochemical analyses were performed on eighteen samples in Activation Laboratories (Ancaster, ON, Canada). REE (Rare Earth Elements) and most of the trace elements were analyzed by Fusion Mass Spectrometry (FUS-MS) (Perkin Elmer Sciex Elan 9000 ICP-MS; Sciex AB, Singapore); Sr, Ba, Zr, and V contents were quantified by Fusion Inductively Coupled Plasma Optical Emission Spectrometry (FUS-ICP) (Varian Vista 735 ICP; Agilent, Santa Clara, CA, USA). Major elements of host rocks, basalts and Cu-mineralized veins were analyzed by FUS-ICP, while contents of iron-rich samples were evaluated with Fusion-X-ray Fluorescence (FUS-XRF) (Panalytical Axios Advanced XRF; PANalytical, Almelo, The Netherlands). FeO was quantified by titration. For samples containing high contents of Mo, Cu, Co. and Ni, analyses were carried out with Fusion Inductively Coupled Plasma Sodium Peroxide Oxidation (FUS-Na_2O_2), and results quantified in percentages rather than in ppm. Afterwards, REE contents were normalized to those of the PAAS (Post Archean Australian Shale; [18]), considered as a reference for sedimentary rocks, while major and trace elements contents have been normalized to those of the UCC (Upper Continental Crust; [18]). Mineralized samples contents have also been compared and normalized with those of host rocks, in order to highlight potential enrichments or depletions in particular elements.

3. Results

3.1. Petrographic Characterization

The Jbel Rhals deposit hosts two types of mineralization located in different veins. On the one hand, Fe-Mn minerals are restrained in decimetric-scaled veins hosted in Paleozoic schists, and overlaid by basalts. On the other hand, Cu minerals are found in veins of millimetric scale cutting Paleozoic schists, Fe-Mn ores, and Triassic conglomerates.

Host rocks and basalts underwent significant fracturing and severe alteration and weathering. Paleozoic schists (Figure 3a) are mainly composed of quartz, muscovite and chlorite; rare single (La, Ce, Nd) phosphate grains are observed associated to quartz (Figure 4f). In some places, the schisteous protolite has been almost completely altered/weathered to clays (probably illite). Triassic conglomerates, composed of quartz and muscovite, experienced a circulation of iron-rich fluids, which turned their original whitish color to a red tint (Figure 5g), and caused the rimming of some quartz grains with goethite. Basalts are strongly altered/weathered: the basalt considered on the field as "the freshest", meaning "poorly weathered", actually lost much of its primary minerals and textures (Figure 3b), while the most altered/weathered one is composed of three layers of different colors and compositions (Figure 3c). In the poorly weathered sample, plagioclase laths are still recognizable, but ferromagnesian minerals are intensively altered/weathered (Figure 3d). Secondary quartz and clays are identified, along with chlorite presenting variable proportions of Al and Fe. Skeletal crystals of ilmenite and hematite, exsolution lamellae of hematite and pyrophanite in ilmenite (Figure 3d,e), and fine hematite dendrites are also observed. Most altered/weathered basalt is composed of a greenish clay-rich layer, a red-brown iron-rich layer and a white layer (Figure 3c,f). The white part is mostly composed of quartz, with some calcite and chlorite (Figure 3h). Quartz, chlorite, clays and calcite are present in the greenish layer, along with some rutile laths (Figure 3g), euhedral apatite and scarce small grains of pyrite. Different grain shapes suggest that some minerals are relics of original/primary ones (Figure 3g), but weathering/alteration made their identification impossible. For instance, the clayey losangic sections observed in Figure 3g are thought to be relics of pyroxenes or olivines. Less common relics are associated to high porosities in the red-brown layer (Figure 3j) where quartz, chlorite, clays, and a mix of calcite, goethite and pyrolusite are identified (Figure 3g). Goethite and pyrolusite are often associated together and form concentric structures, where they are respectively located at the center and at the external rim (Figure 3i). Zircon and (La, Ce, Nd) phosphates have

been observed in the poorly weathered basalt, close to quartz, and in the altered/weathered sample, associated with pyrolusite.

3.1.1. Fe-Mn Mineralization

The main minerals are goethite, hematite and pyrolusite; they are either powdery and poorly crystalline, pseudomorphosing a preexistent rhombohedral mineral (Figure 4b), and/or forming collomorph structures (Figure 4j). Powdery iron oxihydroxides are yellow, red, or even (dark) brown. At Jbel Rhals, rhombohedral goethite sometimes shows a yellow iridescence that is due to a fine layer of iron oxihydroxides coating the surfaces of crystals (Figure 4a). Late sulfates such as jarosite ($KFe_3(SO_4)_2(OH)_6$), melanterite ($FeSO_4 \cdot 7H_2O$) and ferricopiapite ($Fe_5(SO_4)_6O(OH) \cdot 20H_2O$) developed as coatings on the walls and roof of certain galleries (Figure 4l).

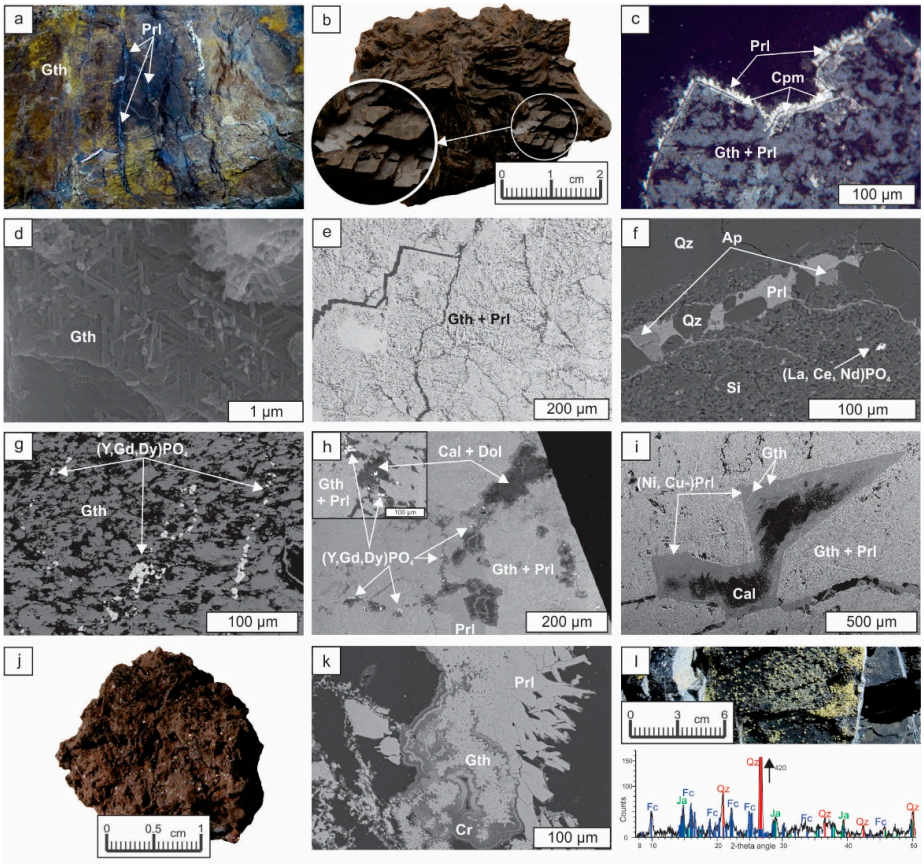

Figure 4. Fe-Mn mineralization (**c**: reflected light photomicrograph; **d**–**i**,**k**: SEM photomicrographs, in backscattered electrons mode). (**a**) Pyrolusite (Prl) veins in iridescent goethite (Gth); (**b**) rhombohedral goethite; (**c**) acicular pyrolusite (Prl) and cryptomelane (Cpm) at the surface of goethite (Gth) intermixed with pyrolusite (Prl); (**d**) goethite (Gth) crystallites highlighting the pseudomorphose of siderite along cleavages; (**e**) cleavages of primary minerals preserved in the intermixed goethite (Gth) and pyrolusite (Prl); (**f**) apatite (Ap) and quartz (Qz) in a pyrolusite (Prl) vein cutting quartz (Qz) and unidentified silicates (Si), where a (La, Ce, Nd) phosphate is observed; (**g**) accumulation of (Y, Gd, Dy)PO_4, in goethite (Gth); (**h**) (Y, Gd, Dy)PO_4 on the edges of calcite (Cal) and dolomite (Dol) crystals, close to pyrolusite (Prl), in the intermixed goethite (Gth) and pyrolusite (Prl); (**i**) calcite (Cal) observed as triangle-shaped sections of rhombohedrons, undergoing weathering and replacement by Ni- and Cu-rich pyrolusite ((Ni, Cu-)Prl) and goethite (Gth), in the intermixed goethite (Gth) and pyrolusite (Prl); (**j**) goethite with collomorph structures; (**k**) pyrolusite (Prl), goethite (Gth), and cryptomelane (Cr) growing in a cavity and forming collomorph structures; (**l**) yellowish jarosite (Ja) and ferricopiapite (Fc) (with X-Ray diffraction pattern) coating the Paleozoic schisteous host rock.

Goethite often shows an unusual habitus denoting the pseudomorphose of a precursor mineral, characterized by rhombohedral dark brown to black crystals (Figure 4b–e), with relatively well-preserved cleavages and fractures often punctuated by Mn oxides. Pyrolusite is often intermixed with goethite (Figure 4c–e), but is also growing as laths on goethite crystals (Figure 4c), and is observed in veins getting through goethite. Other Mn oxihydroxides are noticed, but their identification is difficult due to their common intermixing and small dimensions; we nevertheless suspect the presence of lithiophorite and cryptomelane commonly observed in weathering deposits in Morocco [19] (Figure 4c,k). Quartz is present as large euhedral zones and sometimes as late euhedral crystals growing on goethite and coated by pyrolusite laths. Euhedral apatite is occasionally found in pyrolusite veins (Figure 4f). In the intermixed goethite-pyrolusite, calcite is progressively replaced by Ni- and Cu-rich pyrolusite and goethite, from the outer rim and through cleavages (Figure 4i). Some samples also host collomorph structures involving Fe and Mn (hydr-)oxides (Figure 4j). In most cases, botryoidal goethite grows toward the center of cavities, which are subsequently filled with several generations of pyrolusite laths, goethite needles, and supposed cryptomelane and lithiophorite (Figure 4k). (Y, Gd, Dy) phosphates are evidenced in the powdery, rhombohedral, and collomorph samples, edging some quartz veins, forming "veins" in goethite (Figure 4g) and aggregates close to calcite, dolomite, and pyrolusite (Figure 4h). Very small scarce grains of pyrite and galena have been observed in goethite.

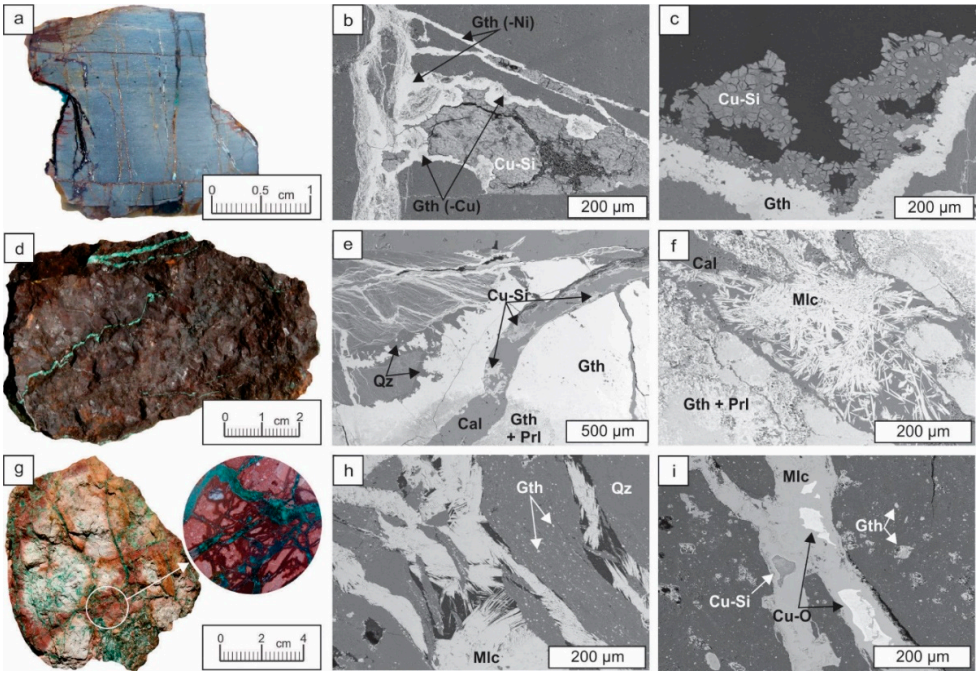

Figure 5. Cu mineralization (**b**,**c**,**e**,**f**,**h**,**i**: SEM photomicrographs, in backscattered electrons mode). (**a**) Cu-veins in Paleozoic schist (polished section); (**b**) hydrated Cu-silicate (Cu-Si) in Ni- or Cu-rich goethite vein (Gth (-Ni) and Gth (-Cu)); (**c**) hydrated Cu-silicate (Cu-Si) covering goethite (Gth); (**d**) Cu-mineralized veins in goethite (and pyrolusite); (**e**) Cu-silicates of various compositions (Cu-Si) in a calcite (Cal) vein cutting quartz (Qz) and the intermixed goethite (Gth) and pyrolusite (Prl); (**f**) acicular malachite (Mlc) in calcite (Cal) vein cutting goethite (Gth) and pyrolusite (Prl); (**g**) Cu-mineralized veins in iron-rich Triassic conglomerate; (**h**) acicular malachite (Mlc) vein cutting through iron-rich conglomerate composed of quartz (Qz) and goethite (Gth); (**i**) hydrated Cu-silicate (Cu-Si) and Cu-oxides (Cu-O) in malachite (Mlc) veins cutting goethite (Gth)-rich conglomerate.

3.1.2. Cu Mineralization

The schisteous basement (Figure 5a,b), the Fe-rich ore (Figure 5d–f) and the Triassic conglomerates (Figure 5g–i) are cut by numerous Cu-mineralized veins. Within schists, veins are mainly filled with

goethite, but malachite and a hydrated Cu-silicate (probably chrysocolla, yet formal identification of this mineral was not possible due to its relative scarcity) are also observed (Figure 5b,c). The veins cutting through goethite and pyrolusite contain calcite, acicular malachite growing from the center to the edges of veins (Figure 5f), and sometimes Cu- (and Ni-) silicates (Figure 5e). Malachite, growing from the edges to the center of veins (Figure 5h), is the main mineral within veins intersecting conglomerates, but cuprite, tenorite, a hydrated Cu-silicate (probably chrysocolla) (Figure 5i), and pyrite relics are noticed at their center.

3.2. Geochemical Characterization

Contents of major, minor or trace, and rare earth elements (REE) of host rocks and mineralizations are presented in Table 1.

3.2.1. Major Element Patterns

Host rocks and mineralizations have similar major element contents (Figure 6a), but Fe_2O_3 and MnO are obviously subject to strong variations. In comparison to the fresh host rock, the altered/weathered schist is slightly depleted in all major elements. Major elements contents of the green part of the altered/weathered basalt are very close to those of the poorly weathered sample, unlike the red part, which is depleted in SiO_2, TiO_2, Al_2O_3, Na_2O, and enriched in Fe_2O_3, MnO, CaO. The fresh host rock, the poorly weathered basalt, and the green altered/weathered basalt are quite rich in their FeO content, which is not the case for the red altered/weathered basalt.

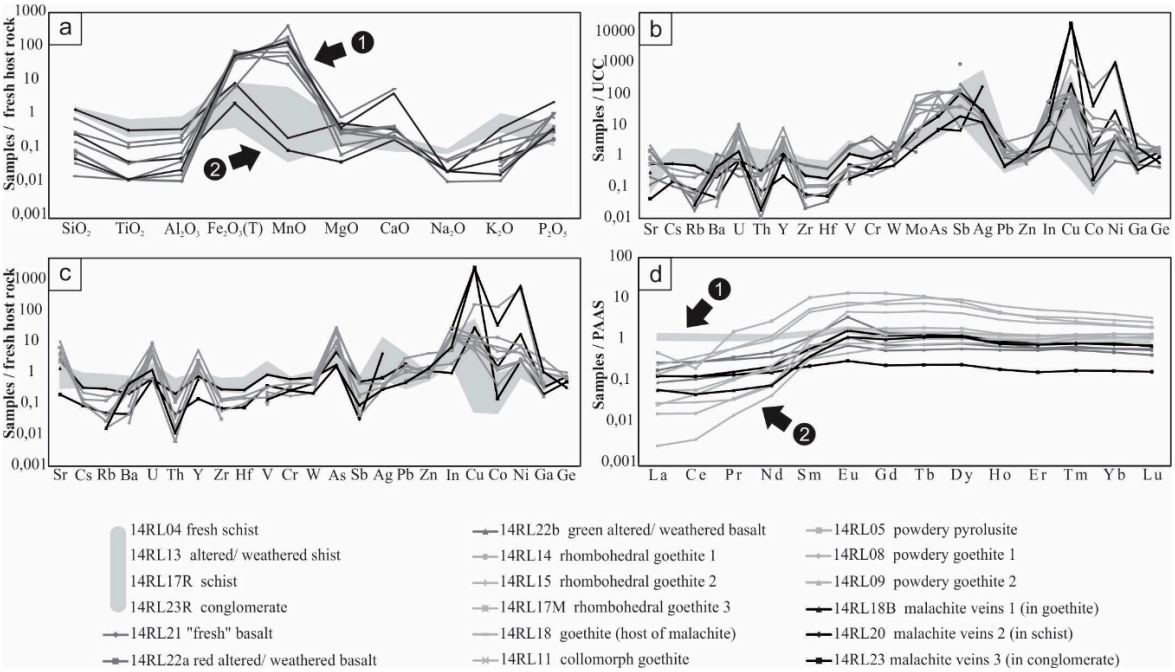

Figure 6. Geochemical data: (**a**) major elements patterns, with values normalized to the host rock (fresh schist). A distinct divergence is observed between the copper veins in schists and conglomerates (group 2), and the others (group 1); (**b**) trace elements patterns, with values normalized to the UCC (Upper Continental Crust) [18]; (**c**) trace elements patterns, with values normalized to the host rock (fresh schist); (**d**) REE patterns, with values normalized to the PAAS [18]. A distinction is observed between the host rocks (no REE fractionation; group 1), and the mineralized samples (REE fractionation; group 2). The shaded areas indicate the major elements (**a**), minor elements (**b**,**c**), and REE (**d**) contents of the host rocks (schists and conglomerate).

Table 1. Results of geochemical analyses for selected samples of host rocks and mineralized samples (W/A = weathered and/or altered). Major elements concentrations are listed in %, minor elements and Rare Earth Elements (REE) are given in ppm. For minor elements, values in bold and marked with an asterisk (*) correspond to contents in %: the detection limit is fixed at 0.01% for Ni and Cu, and 0.001% for Co and Mo. The Eu and Ce anomalies (Eu/Eu* and Ce/Ce*) are calculated with PAAS (Post Archean Australian Shale)-normalized values [18].

		Host Rocks				**Basalts**			**Fe-Mn Mineralization**								**Cu-Mineralization**		
Oxides/Elements	**Detection Limit**	**14RL04 (Fresh Schist)**	**14RL13 (W/A Schist)**	**14RL17R (Host Schist of Goethite)**	**14RL23R (Conglomerate Host of Malachite)**	**14RL21 (Fresh Basalt)**	**14RL22A (Red W/A Basalt)**	**14RL22B (Green W/A Basalt)**	**14RL05 (Powdery Pyrolusite)**	**14RL08 (Powdery Goethite)**	**14RL09 (Powdery Goethite)**	**14RL11 (Collomorph Goethite)**	**14RL14 (Rhombohedral Goethite)**	**14RL15 (Rhombohedral Goethite)**	**14RL17M (Rhombohedral Goethite)**	**14RL18 (Goethite Host of Malachite)**	**14RL18B (Malachite in Goethite)**	**14RL20 (Malachite in Schist)**	**14RL23 (Malachite in Conglomerate)**
Al_2O_3 (%)	0.01	18.84	8.79	15.23	5.00	13.14	0.70	11.86	2.77	3.31	1.32	4.31	0.19	0.30	0.75	0.20	0.41	6.63	0.92
CaO (%)	0.01	0.87	0.07	0.19	0.20	5.57	26.45	2.54	0.19	0.17	0.38	0.26	0.36	0.38	0.16	4.72	3.44	0.30	0.15
Fe_2O_3 (%)	0.01	1.06	0.43	9.08	1.68	4.80	15.76	2.99	6.63	39.15	49.13	44.81	69.85	62.97	75.38	41.79	54.59	8.62	2.16
K_2O (%)	0.01	3.81	2.45	3.82	1.14	0.22	0.05	0.05	0.56	0.68	0.26	0.15	0.04	<0.01	0.08	0.11	0.06	1.44	0.18
MgO (%)	0.01	2.11	0.34	1.22	0.25	5.73	5.37	4.68	0.25	0.71	0.66	0.13	0.54	0.69	0.60	1.67	0.80	1.11	0.08
MnO (%)	0.001	0.156	0.028	0.935	0.006	0.921	4.441	0.279	60.940	7.391	21.220	29.150	10.330	16.150	4.502	23.020	19.840	0.030	0.013
Na_2O (%)	0.01	1.01	0.07	0.09	0.07	2.98	0.05	0.74	0.04	0.04	<0.01	<0.01	0.01	<0.01	<0.01	<0.01	0.02	0.02	0.02
P_2O_5 (%)	0.01	0.17	0.02	0.08	0.03	0.14	<0.01	0.19	0.05	0.13	0.06	0.03	0.17	0.05	0.07	0.18	0.06	0.38	0.03
SiO_2 (%)	0.01	58.13	85.67	65.44	88.22	44.42	16.73	54.21	16.28	39.58	8.86	3.45	4.44	2.02	4.78	0.84	2.77	77.56	14.93
TiO_2 (%)	0.01	0.88	0.53	0.59	0.18	1.07	0.03	0.95	0.09	0.11	0.03	< 0.01	0.01	0.01	0.01	0.01	0.01	0.29	0.03
LOI (%)		4.67	1.59	4.29	2.03	9.79	28.72	6.88	10.45	8.17	12.27	11.66	12.41	12.91	11.36	15.90	11.94	3.14	25.09
Total (%)	0.01	91.70	99.99	100.96	98.81	88.78	98.30	85.37	98.25	99.44	94.19	93.95	98.35	95.48	97.69	88.44	93.94	99.52	43.61
FeO (%)	0.1	6.0	0.1	1.7	<0.1	8.7	<0.1	12.4	<0.1	<0.1	<0.1	<0.1	<0.1	<0.1	<0.1	<0.1	<0.1	2.6	<0.1
V (ppm)	5	142	195	140	333	237	51	197	23	51	48	14	34	18	28	16	20	125	55
Cr (ppm)	20	110	60	80	50	280	30	360	40	50	<20	<20	20	<20	<20	<20	30	70	30
Co (ppm/%)	1	20	1	19	1	19	2	7	53	138	102	277	8	24	30	0.268 *	702	31	3
Ni (ppm/%)	20	70	<20	120	50	70	30	200	490	310	310	530	200	160	170	3.48 *	4.54 *	1230	170
Cu (ppm/%)	10	180	10	150	9480	30	50	190	1600	1860	2790	2530	950	2480	1200	2.92 *	43.9 *	5160	44.5 *
Zn (ppm)	30	70	<30	40	<30	50	<30	40	110	70	70	70	50	80	60	300	100	80	<30
Ga (ppm)	1	29	17	24	8	20	9	20	82	42	12	14	30	10	5	12	32	10	6
Ge (ppm)	1	3	3	3	2	3	1	3	2	3	<1	<1	2	<1	<1	<1	1	2	2
As (ppm)	5	6	<5	9	21	<5	<5	<5	36	138	180	37	168	66	54	124	10	11	28
Rb (ppm)	2	179	117	162	57	7	4	2	23	31	8	5	<2	<2	3	5	3	55	9

Table 1. *Cont.*

Oxides/Elements	Detection Limit	Host Rocks				Basalts			Fe-Mn Mineralization								Cu-Mineralization		
		14RL04 (Fresh Schist)	14RL13 (W/A Schist)	14RL17R (Host Schist of Goethite)	14RL23R (Conglomerate Host of Malachite)	14RL21 (Fresh Basalt)	14RL22A (Red W/A Basalt)	14RL22B (Green W/A Basalt)	14RL05 (Powdery Pyrolusite)	14RL08 (Powdery Goethite)	14RL09 (Powdery Goethite)	14RL11 (Collomorph Goethite)	14RL14 (Rhombohedral Goethite)	14RL15 (Rhombohedral Goethite)	14RL17M (Rhombohedral Goethite)	14RL18 (Goethite Host of Malachite)	14RL18B (Malachite in Goethite)	14RL20 (Malachite in Schist)	14RL23 (Malachite in Conglomerate)
Sr (ppm)	2	74	24	138	57	74	537	43	283	220	776	496	205	339	176	476	105	196	15
Y (ppm)	1/0.5	33	27	35	26	19	24	16	69	179	90	38	61	32	48	88	21	26	5
Zr (ppm)	5	152	84	101	40	94	4	100	19	22	9	<5	<5	<5	5	<5	<5	45	11
Nb (ppm)	1	17	8	9	3	9	5	7	<1	2	<1	<1	<1	<1	<1	<1	<1	3	1
Mo (ppm/%)	2	<2	11	3	7	<2	2	<2	10	64	0.013 *	48	74	64	32	6	3	<2	10
Ag (ppm)	0.5	2.0	3.9	1.3	27.6	1.5	<0.5	1.1	<0.5	<0.5	0.9	0.7	<0.5	<0.5	<0.5	0.6	0.6	8.4	1.4
In (ppm)	0.1	0.1	<0.1	0.2	1.9	0.1	0.8	<0.1	0.2	1.5	3.0	1.8	1.4	1.7	1.5	0.5	0.7	0.1	2.6
Sb (ppm)	0.2	40.7	30.7	2.3	2.7	17.3	179.0	41.4	26.2	28.2	18.5	8.0	22.7	7.2	7.4	1.7	3.8	1.3	21.1
Cs (ppm)	0.5	7.8	3.1	7.6	3.7	0.5	0.9	1.2	1.1	1.8	0.9	<0.5	<0.5	<0.5	<0.5	0.8	<0.5	2.6	0.7
Ba (ppm)	1	527	353	437	151	353	615	142	297	123	148	146	45	13	25	302	243	114	25
Hf (ppm)	0.2	3.9	2.1	2.8	0.9	2.2	0.2	2.3	0.6	0.7	0.4	<0.2	<0.2	<0.2	<0.2	<0.2	<0.2	1.1	0.3
Ta (ppm)	0.1	1.4	1.0	1.1	0.6	0.6	0.2	0.5	<0.1	<0.1	0.3	0.3	<0.1	0.3	0.3	0.3	<0.1	0.6	0.1
W (ppm)	1	4	5	4	4	1	5	2	<1	2	3	2	1	2	3	2	1	3	2
Tl (ppm)	0.1	0.9	0.6	0.7	0.5	0.1	<0.1	<0.1	<0.1	0.8	0.9	1.6	<0.1	0.1	<0.1	0.5	0.7	0.3	<0.1
Pb (ppm)	5	16	65	5	28	15	21	46	19	29	17	26	9	9	8	48	8	<5	30
Bi (ppm)	0.1	0.1	11.8	<0.1	2.1	<0.1	<0.1	<0.1	<0.1	1.0	0.1	<0.1	<0.1	<0.1	<0.1	<0.1	<0.1	<0.1	1.1
Th (ppm)	0.1	16.8	8.8	11.0	3.6	2.4	0.1	2.7	1.9	2.4	0.6	<0.1	<0.1	<0.1	0.3	0.1	0.2	3.6	0.8
U (ppm)	0.1	3.1	6.4	2.3	5.3	0.6	2.1	1.1	27.0	11.8	17.2	11.2	29.3	24.8	11.8	2.0	4.0	2.1	1.9
La (ppm)	0.1	54.7	37.2	41.1	35.8	10.6	6.9	3.5	18.5	9.3	5.5	1.0	0.6	0.1	2.2	1.1	2.3	4.9	5.0
Ce (ppm)	0.1	111.0	77.6	103.0	73.1	23.3	22.4	8.9	16.2	30.7	22.4	3.7	1.3	0.3	4.8	2.4	3.8	10.2	10.3
Pr (ppm)	0.01	12.10	9.37	10.00	8.17	2.95	3.35	1.25	14.10	5.46	5.56	0.94	0.33	0.13	1.04	0.31	0.52	1.48	1.26
Nd (ppm)	0.1	42.3	38.0	39.2	31.7	12.3	15.9	5.8	91.4	31.0	39.3	7.3	2.7	1.4	5.9	2.4	2.5	7.14	5.14
Sm (ppm)	0.1	8.2	8.4	9.1	6.8	3.3	6.4	2.1	59.4	26.5	31.5	6.0	3.0	1.9	4.0	5.5	2.2	3.3	1.3
Eu (ppm)	0.05	1.75	1.77	2.21	1.68	1.26	3.93	0.80	15.10	7.41	8.92	2.05	0.89	0.52	1.18	5.29	1.28	1.85	0.34
Gd (ppm)	0.1	6.6	5.5	8.2	5.0	3.5	7.0	2.6	63.4	41.0	34.8	8.9	3.9	3.0	6.3	21.7	4.8	6.0	1.1
Tb (ppm)	0.1	1.0	0.9	1.3	0.8	0.6	1.0	0.4	8.8	8.1	6.0	1.5	0.8	0.6	1.1	3.8	0.9	1.0	0.2
Dy (ppm)	0.1	6.0	5.1	6.8	4.7	3.6	4.9	2.7	36.4	42.0	29.3	8.3	4.6	3.7	6.7	19.5	5.2	5.6	1.1
Ho (ppm)	0.1	1.1	0.9	1.2	0.8	0.7	0.8	0.6	4.7	6.7	4.4	1.4	1.0	0.8	1.3	3.1	0.8	0.9	0.2

Table 1. *Cont.*

Oxides/Elements	Detection Limit	Host Rocks				Basalts			Fe-Mn Mineralization								Cu-Mineralization		
		14RL04 (Fresh Schist)	14RL13 (W/A Schist)	14RL17R (Host Schist of Goethite)	14RL23R (Conglomerate Host of Malachite)	14RL21 (Fresh Basalt)	14RL22A (Red W/A Basalt)	14RL22B (Green W/A Basalt)	14RL05 (Powdery Pyrolusite)	14RL08 (Powdery Goethite)	14RL09 (Powdery Goethite)	14RL11 (Collomorph Goethite)	14RL14 (Rhombohedral Goethite)	14RL15 (Rhombohedral Goethite)	14RL17M (Rhombohedral Goethite)	14RL18 (Goethite Host of Malachite)	14RL18B (Malachite in Goethite)	14RL20 (Malachite in Schist)	14RL23 (Malachite in Conglomerate)
Er (ppm)	0.1	3.3	2.6	3.4	2.2	1.8	1.8	1.6	9.7	15.6	10.5	3.7	2.9	2.3	3.6	7.5	2.2	2.4	0.5
Tm (ppm)	0.05	0.48	0.39	0.46	0.33	0.28	0.23	0.26	1.13	1.98	1.40	0.51	0.50	0.43	0.55	1.02	0.33	0.34	0.07
Yb (ppm)	0.1	3.2	2.6	2.9	2.1	1.7	1.4	1.7	6.6	11.8	8.4	3.3	3.8	3.2	3.9	6.2	2.3	2.1	0.5
Lu (ppm)	0.01	0.49	0.38	0.43	0.30	0.26	0.18	0.24	0.87	1.47	1.16	0.47	0.59	0.52	0.58	0.85	0.30	0.31	0.07
La/Lu		111.4	99.2	95.1	118.2	41.4	37.6	14.4	21.3	6.3	4.7	2.1	1.0	0.2	3.8	1.3	7.7	15.8	70.0
ΣREE (ppm)		255.2	193.2	232.5	176.2	67.5	80.0	33.1	360.2	246.1	217.5	51.0	27.7	19.4	44.3	85.5	30.6	49.3	27.5
Eu/Eu*		1.12	1.21	1.19	1.34	1.74	2.75	1.62	1.15	1.05	1.26	1.31	1.21	1.02	1.10	2.26	1.84	1.95	1.30
Ce/Ce*		0.99	0.96	1.17	0.98	0.96	1.07	0.98	0.23	0.99	0.93	0.88	0.67	0.60	0.73	0.94	0.80	0.87	0.94

3.2.2. Minor and Trace Elements Patterns

Many values are below the detection limit (e.g., Ta, Nb, Tl, Bi). Host rocks and basalts have higher amounts of Zr and Th than mineralized samples, but are depleted in U, Y, Mo, As, In, Cu, Co., and Ni. The fresh schist, the altered/weathered schist, and gangue minerals of the Fe-Mn mineralization display the highest contents in Rb (respectively 179, 117, and 162 ppm), Nb (respectively 17.3, 7.5, and 9.3 ppm), and Zr (respectively 152, 84, and 101 ppm). Goethite hosting malachite veins is very rich in Cu, Co and Ni (respectively 2.92%, 0.268%, 3.48%), but in this particular case, the enrichment is considered as contamination from the hosted veins during sampling (Figure 5d).

Most samples are enriched in U and depleted in Th, when contents are normalized to those of the UCC (Figure 6b); the more they are rich in U, the less they are in Th. The greenish altered/weathered basalt profile is very similar to that of the poorly weathered basalt, while the red part is more comparable to the mineralized samples. Both altered/weathered basalts are depleted in Co, in comparison to the poorly weathered basalt, but enriched in Cu and Ni. Mineralized samples are enriched in chalcophile elements, but contents in Co and Ni are somewhat variable. All mineralized samples (beside 14RL23), and particularly powdery oxihydroxides, are enriched in Y, as well as goethite 14RL18 reaching 179 ppm. Fe-Mn mineralizations have similar profiles punctuated by enrichments in U, Y, Mo, As, Sb, Ag, In, Cu, Co, Ni, Ga, and depletions in Rb, Ba, Th, Zr, Hf, V, Cr. Cu-mineralized veins have very similar patterns regarding minor elements, but divergent values for Co and Ni. As the fresh host rock only differs from the UCC at the level of Sr, As, Sb, Ag, and Cu, almost no difference is observed between normalization to the schist (Figure 6c) and to the UCC (Figure 6b).

3.2.3. Rare Earth Elements Patterns

Normalization of REE contents of all samples to PAAS (Figure 6d) highlights some significant trends. Host rocks, and more particularly fresh schist, have logically similar flat profiles close to that of the PAAS. All mineralized samples are characterized by a fractionation, with a depletion in LREE (La/Lu between 0.19 and 111.41), but there are significant individual differences between Fe-Mn powdery samples (average La/Lu = 10.78), pseudomorphosing (average La/Lu = 1.57) and collomorph Fe-Mn samples (average La/Lu = 2.13), and Cu veins (average La/Lu = 93.50). Poorly crystalline powdery samples present the highest contents in REE (average ΣREE = 264.82 ppm; five to ten times higher than other samples) and are quite rich in Nd, Gd, Dy, and Sm. Powdery pyrolusite displays a negative Ce anomaly (Ce/Ce* = 0.23).

Both poorly weathered and altered/weathered basalts have similar profiles. In comparison to the poorly weathered basalt, the goethite-rich red altered/weathered sample is enriched in MREE and presents a positive Eu anomaly (Eu/Eu* = 2.75), while the clayey green altered/weathered basalt is depleted in all REE and particularly in LREE. An interesting similarity is noticed between basalts and mineralized samples, particularly the malachite veins: they all show REE fractionation with a slight LREE depletion (respectively, for basalts and the Cu mineralization: average La/Lu = 31.15 and 31.17; ΣREE = 58.16 and 34.66), unlike host rocks (average La/Lu = 105.91 and ΣREE = 211.41). Malachite veins display a very slight positive anomaly in Eu (Eu/Eu* = 1.84, 1.95 and 1.30) similar to basalts, which is not the case of other samples. A division may be observed between malachite veins: those getting through conglomerate are strongly depleted in REE and do not present any fractionation, counter to those cutting goethite and schist showing a slighter depletion.

4. Discussion

As already stressed by many authors, the understanding of supergene deposits formation and the identification of the hypogene ores are complicated by the overprinting of weathering processes over primary ores, and by the lack of data on supergene (and sometimes hydrothermal) fluid chemistry leading to difficulties in quantifying pH, Eh, and geochemical signatures of these fluids. However, as emphasized by [20], textural relations and structures of newly formed mineralizations

allow reasonably accurate deductions about the nature of original minerals and the character of the fresh/unweathered deposits.

At Jbel Rhals, a sequence of mineralization is highlighted by successive intersects of supergene mineralized veins: pyrolusite veins cut through goethite, unidentified silicates and quartz veins go through goethite and pyrolusite, and fine calcite and malachite veins pass through goethite, pyrolusite and silicates. Goethite is the first supergene minerals to precipitate; pyrolusite (probably followed by lithiophorite and cryptomelane) forms later, under more oxidizing conditions (Figure 7). The Fe-Mn oxihydroxides forming rhombohedral minerals seem to replace a primary mineral, thought to be a carbonate (probably siderite—see below). Their precipitation is followed by the filling of cavities and fractures with minerals forming collomorph structures, and finally by poorly crystalline powdery minerals. Malachite, calcite, and probably chrysocolla precipitate later, in thinner veins that cross through Fe-Mn ores. Sulfates observed on some walls formed recently, and most probably are related to ongoing mining activities.

4.1. Hydrothermal Alteration and/or Weathering of Basaltic Rocks

The Jbel Rhals host rocks, especially basalts, show evidence of extensive alteration and/or weathering, as attested by the various secondary products, the few preserved primary minerals (Figure 3d–g), and the mineralogical and chemical variation of the layered most altered/weathered basalt (Figure 3c). Some secondary minerals may result from low-temperature hydrothermal alteration (e.g., chlorite, albite and clays), while others from weathering processes (e.g., goethite and pyrolusite), but mixing of these mineral phases get the determination even more complicated in terms of origin, and the understanding of their formation processes more complex.

Weathering of basalts usually follows the next sequence: glass–plagioclases–ferromagnesian minerals—Fe and Ti oxides [21,22]. When the glass proportion is significant, that component being particularly susceptible to weathering, the weathering sequence is modified as follows: glass–ferromagnesian minerals–plagioclases–Fe and Ti oxides [23,24]. Plagioclases and Fe-Ti oxides are the only primary minerals remaining in Jbel Rhals basalts (Figure 3d), which suggests that weathering followed the second sequence described above. Preservation of Fe-Ti oxides during weathering is quite common, as observed by [21,25]. The relatively close TiO_2 contents of the greenish layer and the parent basalt endorse that Ti-oxides tend to be immobile during weathering of Jbel Rhals ore and that they were moderately dissolved and transported [25–27]. Exsolution lamellae of hematite (and pyrophanite) in ilmenite are primary, and the skeletal shape of crystals reflects their fast growth under supercooling (Figure 3e).

The layered structure of the altered/weathered basalt (Figure 3c) and the mineralogical and geochemical segregation in the three layers (Figure 3f) suggest a sequential weathering of primary minerals and reflect various environments of precipitation. The red layer, rich in Fe^{3+}, Mn, Ca, and mobile elements such as U (Figure 6, Table 1), is mostly composed of goethite and pyrolusite (Figure 3h–j) that may result from alteration/weathering of ferromagnesian minerals such as pyroxenes and olivines [21,28,29]. The greenish layer, composed of quartz, calcite, chlorite, clays (Figure 3g) and rich in Si and Al (Table 1), is thought to concentrate alteration/weathering products of the dissolution of feldspars [21,28,29], and (relics of) primary minerals, resulting in a relative enrichment in immobile elements (e.g., Th, Zr, Ti). Chlorite and clays are typical features of the hydrothermal alteration of basalts, and are here frequently observed as pseudomorphs after primary minerals, as stressed by [29,30]. Albite is thought to be formed from the low-temperature hydrothermal alteration of anorthite. The conservation of original minerals fabrics and the filling of spaces created by dissolution with associated clays and Fe oxihydroxides (Figure 3h,j) imply that the alteration/weathering took place under isovolumetric conditions [31,32]. The various undetermined and mixed silicates observed in veins cutting through schist and Fe-Mn mineralization are also thought to be the result of the alteration/weathering of basalts and from the percolation of derived fluids [30]. The white layer is

made of quartz (Figure 3h,i) that precipitated later than minerals of the two other layers, from Si-rich fluids circulating through voids fractures, probably under acidic conditions.

The geochemical features (REEs, major and minor elements) of the greenish layer are very close to those of the parent basalt, which is not the case of the red part (Figure 6). The latter is much closer in composition to the Fe-Mn mineralization. This variance reflects the successive steps of weathering of the primary minerals, the subsequent partition of elements, and their precipitation into specific mineral phases, under particular conditions. Respectively, the very low and slightly high FeO contents of the red and greenish layers also indicate that minerals of the red part formed under oxidizing conditions, while reducing conditions prevailed during precipitation in the greenish layer. The (slight) positive Eu anomalies of basalts, and especially of the red altered/weathered layer, are related to the decoupling of Eu from other REE, because of its presence as trivalent (under surface conditions) or divalent (in reduced environments and at elevated temperatures and pressures) cations [33,34]. The positive anomaly of the poorly weathered basalt is related to the incorporation of Eu in plagioclase during magmatic processes [35]. As plagioclase is absent from most altered/weathered layers, Eu is supposed to be incorporated in a secondary phase, hydrothermal or supergene, by adsorption on clay minerals and/or co-precipitation with Fe oxihydroxides [33,36,37]. According to [30,34,37,38], positive Eu anomalies related to the predominance of Eu^{2+} in hydrothermal fluids are indeed typically found in associated ore deposits.

4.2. Fe-Mn Mineralization

The unusual rhombohedral crystals of Jbel Rhals goethite denote the pseudomorphosis of a former mineral. This hypogene mineral is thought to be siderite, although this mineral has not been observed at Jbel Rhals, probably owing to the high degree of weathering and the extreme instability of this mineral under oxidizing conditions (Figure 7a) [39]. Pseudomorphosis of goethite and pyrolusite after siderite is common in supergene environments [20,39] and has been documented in many places, e.g., at Akjouit (Mauritania; [20]), Lake George (USA; [40]), Errachidia (Morocco; [41]), Ljubija (Bosnia; [42]), Schwarzwald (Germany; [43]), and Granada (Spain; [44]). Besides the rhombohedral characteristic of the pseudomorphs, other diagnostic indications of the initial presence of siderite at Jbel Rhals are cleavages, the Mn content, and the dark-brown color. Relatively well-preserved 120°-orientated cleavages and fractures of the primary carbonate are forming a "box-work pattern" (Figure 4d) and are punctuated with goethite and pyrolusite, as described by [40] in Colorado (USA). The intermixing of goethite and pyrolusite, the development of pyrolusite laths at the surface of goethite and quartz crystals, in cavities and veins cutting goethite, also support the hypothesis of primary siderite at Jbel Rhals. Siderite usually contains a significant amount of Mn (1–3%) that can be released during weathering and be available for later Mn oxides formation [31,42]. The close association of goethite and pyrolusite is thus related to the release of the Mn that crystallizes as small aggregates of pyrolusite arranged within the network of goethite [44]. The supposed hypogene siderite is probably of hydrothermal origin: siderite typically forms in reduced environments from solutions containing little dissolved sulfur but a lot of bicarbonate ions [39]. Some small scarce sulfide grains such as chalcopyrite, pyrite, and galena, observed in the ore, are strengthening this hypothesis, as hydrothermal siderite is commonly accompanied by such sulfides as that concentrate the little dissolved sulfur present in solution [39,45,46].

Goethite is the most common and most stable Fe oxihydroxide under atmospheric conditions (Figure 7a), and is widely observed in gossan of ore deposits. Hematite, present in minor proportions at Jbel Rhals, is thought to have precipitated shortly before goethite but to have turned into goethite as the latter is more stable under oxidizing conditions (Figure 7a). It is also possible, but quite unlikely, that hematite formed during hydrothermal processes, and that small amounts have been preserved from weathering. Large euhedral quartz is supposed to have formed during hydrothermal phases. The fine quartz veins cutting mineralization and basalts, and the small crystals observed at the surface of various minerals precipitated during the last stages of weathering.

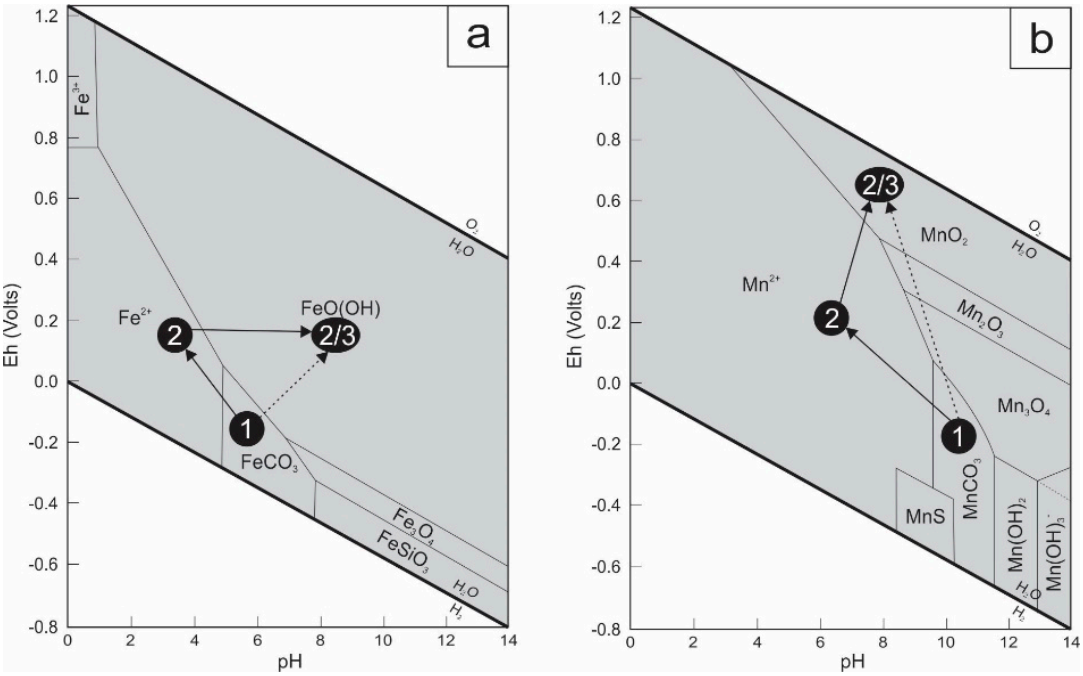

Figure 7. (**a**) Eh–pH diagram for a part of the Fe-C-Si-O-H system, showing the stability fields of selected iron minerals at 25 °C and 1 atmosphere (modified after [47]). Siderite (1) may be directly weathered in goethite (2), or it may be leached first, leading to the presence of aqueous Fe^{2+} (2) and later to the precipitation of goethite (3); (**b**) Eh–pH diagram for a part of the Mn-C-S-O-H system showing the stability fields of selected manganese minerals at 25 °C and 1 atmosphere (modified after [47]). Rhodochrosite may be directly weathered in pyrolusite (2), or is firstly leached, leading to the presence of aqueous Mn^{2+} (2) and later to the precipitation of pyrolusite (3).

In supergene environments, manganese oxide minerals are represented by pyrolusite, cryptomelane, todorokite, nsutite, and other poorly defined phases [19,48–50]. Pyrolusite, which is only stable under strongly oxidizing conditions and at neutral to basic pH (Figure 7b), is the most common Mn oxide at Jbel Rhals. Two generations of pyrolusite are recognized: the first precipitated with goethite, in pseudomorphose of siderite (Figure 4b–e), while the second formed later, during the last stages of weathering, at the surface of goethite crystals (Figure 4c), in cavities, and in veins cutting through goethite. Such early and late pyrolusite have already been observed in the Mn Imini district, 500 km southwestward [19]. Collomorph structures filling cavities and including goethite, pyrolusite and cryptomelane (Figure 4j,k) are thought to be contemporary of the second generation of pyrolusite, and to have precipitated from successive generations of supergene fluids of various compositions with increasing O_2 content to allow Mn(IV) in the form of pyrolusite. The small amount of these structures does not allow further conclusions about their genesis to be drawn. Later precipitation of Mn oxides, in comparison to Fe oxihydroxides, is due to the greater solubility of Mn in oxidizing fluids, and to its greater resistance to oxidation. The presence of Mn oxides (particularly pyrolusite) suggests that highly oxidizing conditions were reached, particularly in the vicinity of fissures and cavities [51].

Enrichment in U but depletion in Th of the Fe-Mn mineralized samples, in comparison to host rocks and basalts of Jbel Rhals (Figure 6b,c), is a typical supergene trend and is related to a selective U vs. Th mobilization during weathering processes. Soluble and mobile U in supergene fluids is preferentially leached and accumulated in neoformed minerals (oxihydroxides), while immobile Th is retained in weathering-resistant minerals or incorporated in rapidly precipitating minerals [52–55]. The concentration of U in Fe-Mn oxihydroxides and clays is related to the high specific surface of these minerals and the subsequent important adsorption capacity [56], but also to the neoformation of discrete minerals at the interface between Fe-Mn oxihydroxides and clays, and fluids [51,53,54,57].

In the same trend, host rocks are rich in immobile Zr, Rb, Nb, while mineralized samples are rich in Y, Mo, As, Sb, In, and chalcophile elements that may be adsorbed on Fe-Mn oxihydroxides (as observed in other Fe-Mn mineralization; [58]) and clays or incorporated into supergene minerals. Enrichment of As is related to the adsorption of this element by Fe oxihydroxides, in the form of arsenate or $FeAsO_4$, in oxic environments [36,59].

The slightly negative Ce anomaly of poorly crystalline pyrolusite is the only noteworthy feature observed in Figure 6d. Ce anomaly results from oxidation of this element to Ce^{4+} and to its subsequent decoupling from the other REE which maintain their trivalent ionic states and are leached by circulating water [60]. Oxidation to Ce^{4+} is restricted to strongly oxidizing environments, and is usually observed in the most weathered part of the profiles, for Fe-Mn oxihydroxides patterns [24,48,61]. The lack of a general negative Ce anomaly at Jbel Rhals might indicate that the tetravalent Ce was incorporated in other mineral phases than pyrolusite, or that pyrolusite precipitated under unusually low pH conditions, as Ce^{4+} is unstable below pH 4 and 5 [37,47].

The low-grade enrichment in REE and the preferential intake of HREE+Y (Figure 6) of Fe-Mn oxihydroxides are typical features of supergene deposits associated to igneous rocks [25,62] and have been correlated with the presence of secondary phosphates close to weathered basalts in French Polynesia [61] and in Hawaii [63]. The highest REE + Y content of the amorphous, poorly crystalline, powdery Fe oxihydroxides (Figure 6) is related to (1) the trapping of (M)REE by these minerals, under acid conditions, by coprecipitation and adsorption processes [64,65], (2) the sorption of REE onto the surface of clays that are common in powdery samples [66,67], (3) the presence of (Y, Gd, Dy) phosphates in the ore. The occurrence of multiple REE, whether La-Ce-Nd or Y-Gd-Dy (Y being usually considered with HREE to which it is chemically and physically similar), within a single mineral, is due to the similar ionic radii and trivalent oxidation state of these elements, and to the subsequent common substitution of REE for each other into crystal structures [62]. The origin of REE may be the dissolution of minerals observed in the parent rock (monazite, allanite, . . .), or the release of trace concentrations present in primary and/or hydrothermal apatite, calcite, dolomite, feldspars, . . . , [62,66,68]. Here, MREE enrichment suggests that REEs originate from the weathering of primary phosphate minerals, and particularly of apatite [69,70]. (La, Ce, Nd) phosphates are only observed in host rock (Figure 4f) and basalts, close to primary minerals, and are therefore supposed to be primary minerals that resisted weathering [66]. The low mobility of LREE may also have caused the rapid precipitation of LREE phosphates, close to parent rocks, while more mobile HREE were more importantly leached [71,72]. The proximity of (Y, Gd, Dy) phosphates with Fe-Mn ore (Figure 4g), quartz veins, calcite, pyrolusite and cavities (Figure 4h) suggests that these minerals are supergene, in agreement with the observations of [68,72,73], suggesting that HREE phosphates are generally concentrated in fissure fillings and voids, along with minerals precipitating during the late stages of weathering.

4.3. Cu Mineralization

The small amount of Cu mineralization in veins does not allow extensive conclusions about their genesis to be drawn. Goethite, malachite, chrysocolla, and Cu-oxides are observed in veins cutting through the Paleozoic schisteous basement (Figure 5a–c), the intermixed goethite-pyrolusite (Figure 5d–f), and Triassic conglomerates (Figure 5g–i). Textures and sequences highlighted in these veins suggest that these minerals are of supergene origin. Cu-oxides and hydrated silicates (Figure 5i) formed prior to and later than malachite, respectively; euhedral malachite needles precipitated prior to calcite, which is filling the cavities (Figure 5f). Goethite precipitated in these veins before Cu-minerals (Figure 5b), but is younger than the Fe-Mn intermixed ore. Late precipitation of carbonates indicates that during most of the weathering, acid conditions hindered the formation of these phases, and that higher pH values were only reached during the latest stages. The source of Cu may be Cu-sulfides that formed during hydrothermal processes, and were rapidly weathered to malachite, oxides and silicates when Eh increased. Some scarce grains of strongly weathered pyrite and the occurrence of Ni-rich goethite strengthen the hypothesis that Cu-, Fe- (and Ni-) sulfides existed in the primary ore.

The similar REE, major and minor elements patterns of the Cu and Fe-Mn mineralization (Figure 6) may imply that the precipitation of these phases is related to the same supergene event(s); Fe and Mn were mobilized and precipitated during the first stages of supergene precipitation, while chalcophile elements remained in solution and precipitated later. The geochemical differences between the veins cutting schists and goethite, and those cutting conglomerates, notably for Co. and Ni contents (Figure 6), suggest that two generations of Cu-mineralized veins are present at Jbel Rhals. Veins cutting through conglomerates are thought to have formed later. Their REE pattern shows no fractionation, close to the host conglomerate, and their depletion in Y contrasts with other mineralized samples, confirming this hypothesis (Figure 6c,d).

4.4. Late Sulfates

Late sulfates (jarosite, melanterite and ferricopiapite) developed locally as coatings on galleries walls and roofs (Figure 4l) are supposed to be recent and related to mining activities. Their occurrence may indicate the initial presence of pyrite that would have been destabilized by strongly acid conditions prevailing at a very local scale.

4.5. Metallogenic Model of Formation

The textural, mineralogical and geochemical observations listed above suggest that the studied rocks underwent several episodes of transformation, and that the various minerals observed in the ores result from weathering events superimposed on hydrothermal altered rocks and hydrothermal siderite-based metal sulfide veins (Figure 8). The polyphased metallogenic history of Jbel Rhals polymetallic deposit is characterized by (1) the circulation of hydrothermal fluids shortly after the basalts flows, which triggered some hydrothermal alteration and the precipitation of associated minerals, and (2) the later circulation of oxidizing fluids that activated weathering of the ores and their environment (Figure 8). The presence of basalts, whose Permian/Triassic flow are related to the Central Atlantic Magmatic Province (CAMP), supports the hypothesis of early hydrothermal ore formation at Jbel Rhals [46]. The hydrothermal hypogene ores are then considered to be late Permian to Triassic in age and to have been induced by the thermal heat flow and events triggered by the Permian-Triassic rifting of the Central Atlantic, just as suggested in other mineral deposits of North Africa [29,74–77]. Among multiple outcomes, these hydrothermal processes may be responsible for the alteration of basalts, and for the formation of secondary phases such as chlorite and clays, siderite and sulfides. Altered rocks and mineralizations were later subjected to supergene processes that are probably related to the Cenozoic High Atlas orogeny. Several episodes of uplift (defined by [5,6,16]) generated the exhumation of series and ores and promoted their exposition to oxidizing atmospheric conditions and meteoric water, leading to their weathering. Intense fracturing of host rocks facilitated infiltration and percolation of mineralizing fluids, which were in addition not hindered by the previously altered basalt. The lack of carbonates in the host rocks prevented buffering of the fluids acidity and led to the precipitation of minerals stable under acidic conditions, such as goethite. Fe-Mn oxihydroxides precipitated first, and were later cut by Cu-mineralized veins.

The origin of metals is a matter of debate, since potential repeated mobilization and reprecipitation of minerals during hydrothermal and supergene processes surely overprinted initial features of the ores. Paleozoic schists clearly underwent alteration and weathering, as attested by the presence of clay and chlorite in some samples, but the lack of geochemical similitudes with ores does not support the hypothesis of their unique contribution to mineralization formation. Triassic conglomerates have been affected by weathering, as indicated by the formation of interstitial goethite and malachite in veins. Jbel Rhals basalts have been subjected to successive hydrothermal and supergene processes that undoubtedly modified the equilibrium of underneath formations, caused the input of chemical elements in underlying rocks, and had an important role in the subsequent formation of mineralizations. As suggested by [28] in other places than Jbel Rhals, it is plausible that fluids emanating from the alteration and weathering of the basalts contributed to the formation of some hydrothermal

and supergene mineral phases. Interesting geochemical similarities noticed between basalts and mineralized samples support this hypothesis: they both show REE fractionation, slight LREE depletion, and enrichment in MREE, which is not the case of the schisteous host rocks (Figure 6). The Co- and Ni-rich signature of most mineralized samples (Figure 6) also supports the hypothesis that basaltic rocks influence ore formation, as described elsewhere [58]. Clays and chlorite precipitation is considered to be related to feldspars alteration/weathering. Siderite and sulfides, goethite and hematite, formed under respectively reduced (hydrothermal) or oxidized (supergene) conditions, are thought to be related to the alteration/weathering of ferromagnesian minerals that may release large quantities of Fe [28,31]. Basalts are therefore regarded as one of the metal sources at Jbel Rhals, other sources being for instance the altered/weathered host rocks.

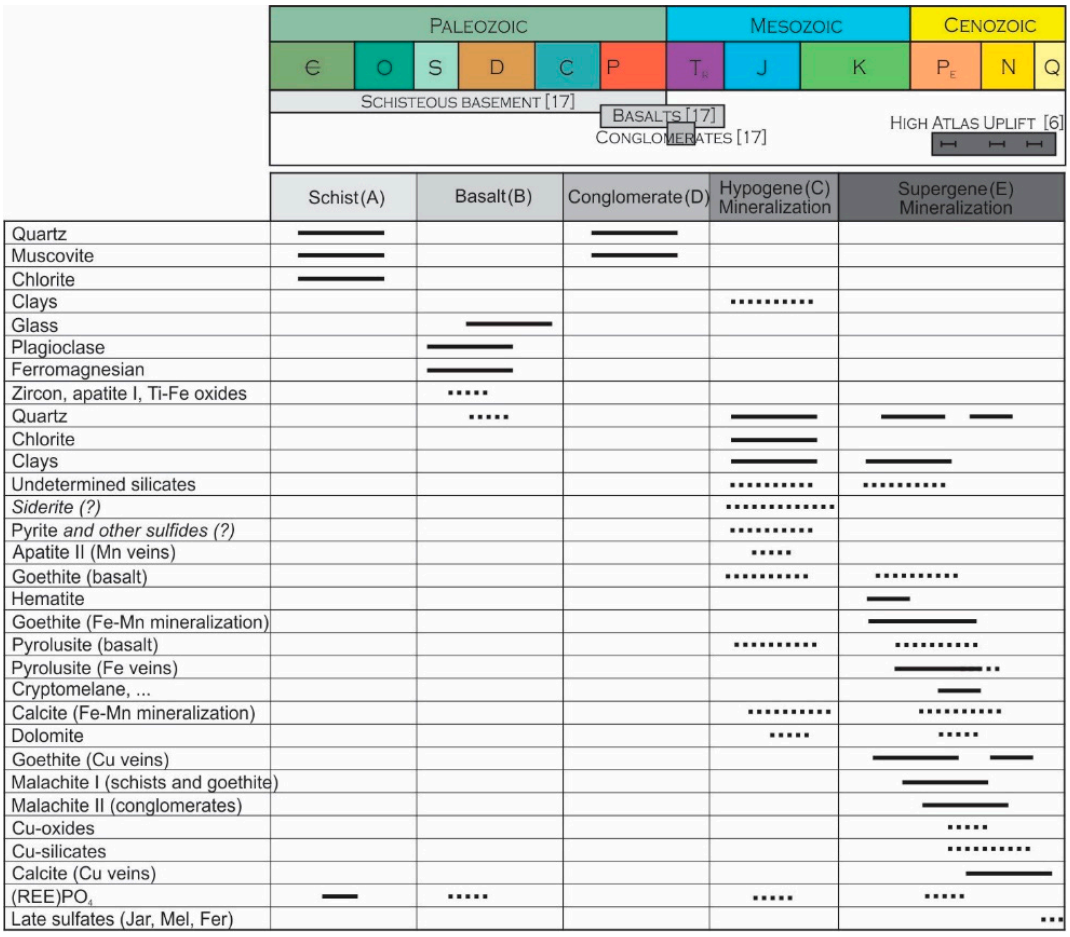

Figure 8. Paragenese of Jbel Rhals rocks and mineralizations, in relation to the evolution of the geological/geodynamical context: (**A**) formation of the Paleozoic schisteous basement; (**B**) Permo-Triasic basalts flow; (**C**) alteration of the host rocks, basalts, and formation of a hydrothermal ore; (**D**) Triassic conglomerates; (**E**) weathering probably related to the High Atlas Uplift. Relative ages of the formations are from [4], and of the High Atlas uplift from [6].

5. Conclusions

The Jbel Rhals polymetallic deposit has a polyphased metallogenic history, with mineralization resulting from supergene processes superimposed over hydrothermal alteration. The supergene phases constitute the major mineralization currently observed (goethite, hematite, pyrolusite, cryptomelane, malachite, Cu-oxides and silicates, calcite, dolomite, REE(PO_4), late sulfates, quartz, clays, silicates) whereas little is left of the hydrothermal mineralization (siderite and minor sulfides). The flow of basalts into the Paleozoic schisteous basement, during Permian-Triassic, the subsequent circulation

of hydrothermal fluids through basalts and host rocks, and the formation of the primary deposit, are related to the same geotectonic settings that are part of the intracontinental rifting stage. These hydrothermal processes triggered the alteration of schists and basalts, the leaching of some elements as iron from rocks through fluid–rock interaction, and the formation of a hydrothermal mineral assemblage presumably composed of siderite and sulfides that precipitated from high temperature fluids. During the Cenozoic Era, several episodes of uplift recorded in the High Atlas enabled the exhumation of basalts, host rocks, and hypogene ores, their subsequent weathering, and the formation of a supergene ore from oxidizing low temperature surface-derived fluids. Hydrothermal siderite has thereby been replaced, sometimes "in situ", by Fe-Mn oxihydroxides (goethite, pyrolusite), while dissolved sulfides were notably later involved in the malachite formation. These supergene processes are also related to the enrichment in HREE, Y, and mobile elements such as U in secondary minerals.

Acknowledgments: Michèle Verhaert thanks the Belgian Fund For Scientific Research (FNRS), for providing her with a FRIA PhD grant. We thank the administration of Bou Arfa for field access and facilities to the mines. Many thanks are due to Gaëtan Rochez (UNamur) for the field support and pictures. Ludovic Lafforgue is thanked for his help on the field. We also express our gratitude to the reviewers for their constructive comments that significantly improved the manuscript.

Author Contributions: M.V., O.S., A.D., and J.Y. took part to the field campaigns. M.V. performed the experiments, analyzed and discussed the results, and wrote the paper. A.B. and O.S. facilitated the experiments. A.D. and M.E. took part to the discussion. J.Y. coordinated the study.

Conflicts of Interest: The authors declare no conflict of interest.

References

1. Verhaert, M.; Bernard, A.; Dekoninck, A.; Yans, J. Characterization and genesis of Cu-Pb-Zn-V-Fe-Mn supergene ore deposits in the area of Bou Arfa (Oriental High Atlas, Morocco). *Geol. Belg.* **2016**, *19*, 303–304.
2. Verhaert, M.; Bernard, A.; Dekoninck, A.; Lafforgue, L.; Saddiqi, O.; Yans, J. Mineralogical and geochemical characterization of supergene Cu–Pb–Zn–V ores in the Oriental High Atlas, Morocco. *Miner. Depos.* **2017**, *52*, 1049–1068. [CrossRef]
3. Lafforgue, L. Place de la Minéralisation de Manganèse de Bou Arfa Dans L'évolution Méso-Cénozoïque de L'oriental Marocain. Ph.D. Thesis, University Paris-Saclay, Orsay, France, 2016.
4. Chefchaouni, Y.C.; Diouri, M.; Choubert, G. Carte géologique du Haut Atlas oriental, feuilles Bou Arfa, Iche, Talzaga et Figuig. *Notes Mémoires Serv Géol. Maroc* **1963**, *158*.
5. Frizon de Lamotte, D.; Zizi, M.; Missenard, Y.; Hafid, M.; El Azzouzi, M.; Maury, R.; Charriere, A.; Taki, Z.; Benammi, M.; Michard, A. The Atlas System. In *Continental Evolution: The Geology of Morocco: Structure, Stratigraphy, and Tectonics of the Africa-Atlantic-Mediterranean Triple Junction*; Michard, A., Ed.; Springer: Heidelberg, Germany, 2008; pp. 133–202, ISBN 3540770755.
6. Leprêtre, R.; Missenard, Y.; Saint-Bezar, B.; Barbarand, J.; Delpech, G.; Yans, J.; Dekoninck, A.; Saddiqi, O. The three main steps of the Marrakech High Atlas building in Morocco: Structural evidences from the southern foreland, Imini area. *J. Afr. Earth Sci.* **2015**, *109*, 177–194. [CrossRef]
7. Teixell, A.; Arboleya, M.L.; Julivert, M.; Charroud, M. Tectonic shortening and topography in the central High Atlas (Morocco). *Tectonics* **2003**, *22*, 1051–1064. [CrossRef]
8. Laville, E.; Pique, A.; Amrhar, M.; Charroud, M. A restatement of the Mesozoic Atlasic Rifting (Morocco). *J. Afr. Earth Sci.* **2004**, *38*, 145–153. [CrossRef]
9. El Kochri, A.; Chorowicz, J. Oblique extension in the Jurassic trough of the central and eastern High Atlas (Morocco). *Can. J. Earth Sci.* **1995**, *33*, 84–92. [CrossRef]
10. Sarih, S. Géodynamique et Transferts Sédimentaires des Bassins Liasiques Du Haut-Atlas Central (Maroc). Ph.D. Thesis, University of Bourgogne, Dijon, France, 2008.
11. Mattauer, M.; Tapponnier, P.; Proust, F. Sur les mécanismes de formations des chaines intracontinentales. L'exemple des chaines atlasiques du Maroc. *Bull. Soc. Geol. Fr.* **1977**, *7*, 521–526. [CrossRef]
12. Giese, P.; Jacobshagen, V. Inversion tectonics of intracontinental ranges: High and Middle Atlas, Morocco. *Geol. Rundsch.* **1992**, *81*, 249–259. [CrossRef]

13. Knight, K.B.; Nomade, S.; Renne, P.R.; Marzoli, A.; Bertrand, H.; Youbi, N. The Central Atlantic Magmatic Province at the Triassic-Jurassic boundary: Paleomagnetic and 40Ar/39Ar evidence from Morocco for brief, episodic volcanism. *Earth Planet. Sci. Lett.* **2004**, *228*, 143–160. [CrossRef]
14. Youbi, N.; Martins, L.T.; Munhá, J.M.; Ibouh, H.; Madeira, J.; Aït Chayeb, E.H.; El Boukhari, A. The Late Triassic-Early Jurassic Volcanism of Morocco and Portugal in the Framework of the Central Atlantic Magmatic Province: An Overview. In *The Central Atlantic Province; Insights from Fragments of Pangea*; Hames, W.E., McHone, J.G., Renne, P.R., Ruppel, C., Eds.; American Geophysical Union: Washington, DC, USA, 2003; pp. 179–207, ISBN 9781118668771.
15. Laville, E.; Piqué, A. La distension crustale atlantique et atlasique au Maroc au début du Mésozoïque: Le rejeu des structures hercyniennes. *Bull. Soc. Geol. Fr.* **1991**, *162*, 1161–1171.
16. Frizon de Lamotte, D.; Saint Bezar, B.; Bracène, R.; Mercier, E. The two main steps of the Atlas building and geodynamics of the Western Mediterranean. *Tectonics* **2000**, *19*, 740–761. [CrossRef]
17. Missenard, Y.; Zeyen, H.; de Lamotte, D.F.; Leturmy, P.; Petit, C.; Sébrier, M.; Saddiqi, O. Crustal versus asthenospheric origin of relief of the Atlas mountains of Morocco. *J. Geophys. Res.* **2006**, *111*, 1–13. [CrossRef]
18. Taylor, S.R.; McLennan, S.M. *The Continental Crust: Its Composition and Evolution; an Examination of the Geochemical Record Preserved in Sedimentary Rocks*; Blackwell Scientific Publications: Oxford, UK, 1985; ISBN 0632011483.
19. Dekoninck, A.; Bernard, A.; Barbarand, J.; Saint-Bezar, B.; Missenard, Y.; Lepretre, R.; Saddiqi, O.; Yans, J. Detailed mineralogy and petrology of manganese oxyhydroxide deposits of the Imini district (Morocco). *Miner. Depos.* **2016**, *52*, 1049–1064. [CrossRef]
20. Ramdohr, P. *The Ore Minerals and Their Intergrowths*; Pergamon Press, Ed.; Pergamon Press: Oxford, UK, 1980; ISBN 9780080116358.
21. Dekayir, A.; El-Maataoui, M. Mineralogy and geochemistry of supergene alteration of an alkali basalt from the Middle Atlas, Morocco. *J. Afr. Earth Sci.* **2001**, *32*, 619–633. [CrossRef]
22. Macaire, J.; Perruchot, A. Transformations Géochimiques au Cours de l'Altération Météorique d'une Basanite Pliocène du Massif Central Français. *Geoderma* **1988**, *41*, 287–314. [CrossRef]
23. Karrat, L.; Perruchot, A.; Macaire, J.J. Weathering of a quaternary glass-rich basalt in Bakrit, Middle Atlas Mountains, Morocco. *Geodin. Acta* **1998**, *11*, 205–215. [CrossRef]
24. Ludden, J.N.; Thompson, G. An evaluation of the behavior of the rare earth elements during the weathering of sea-floor basalt. *Earth Planet. Sci. Lett.* **1979**, *43*, 85–92. [CrossRef]
25. Nesbitt, H.W.; Wilson, R.E. Recent chemical weathering of basalts. *Am. J. Sci.* **1992**, *292*, 740–777. [CrossRef]
26. Maulana, A.; Yonezu, K.; Watanabe, K. Geochemistry of rare earth elements (REE) in the weathered crusts from the granitic rocks in Sulawesi Island, Indonesia. *J. Earth Sci.* **2014**, *25*, 460–472. [CrossRef]
27. Sanematsu, K.; Moriyama, T.; Sotouky, L.; Watanabe, Y. Mobility of Rare Earth Elements in Basalt-Derived Laterite at the Bolaven Plateau, Southern Laos. *Resour. Geol.* **2011**, *61*, 140–158. [CrossRef]
28. Daoudi, L.; Pot de Vin, J.L. Effets thermique et hydrothermal de la coulée de basalte triasico-liasique sur les argiles du bassin d'Argana (Maroc). *C. R. Geosci.* **2002**, *334*, 463–468. [CrossRef]
29. Kamel, S.; Bouabid, R.; Boulangé, B.; Colin, F. Paléoaltérations hydrothermale et supergène dans un basalte triasique du Moyen Atlas, Maroc. *J. Afr. Earth Sci.* **1996**, *23*, 225–235. [CrossRef]
30. Torres-Alvarado, I.S.; Pandarinath, K.; Verma, S.P.; Dulski, P. Mineralogical and geochemical effects due to hydrothermal alteration in the Los Azufres geothermal field, Mexico. *Rev. Mex. Cienc. Geol.* **2007**, *24*, 15–24.
31. Hamidi, E.M.; Boulangé, B.; Colin, F. Altération d'un basalte triasique de la région d'Elhajeb, Moyen Atlas, Maroc. *J. Afr. Earth Sci.* **1997**, *24*, 141–151. [CrossRef]
32. Morey, G.B.; Setterholm, D.R. Rare earth elements in weathering profiles and sediments of Minnesota: Implicatinos for provenance studies. *J. Sediment. Res.* **1997**, *67*, 105–115. [CrossRef]
33. Lewis, A.J.; Palmer, M.R.; Sturchio, N.C.; Kemp, A.J. The rare earth element geochemistry of acid-sulphate and acid-sulphate-chloride geothermal systems from Yellowstone National Park, Wyoming, USA. *Geochim. Cosmochim. Acta* **1997**, *61*, 695–706. [CrossRef]
34. Sverjensky, D.A. Europium redox equilibria in aqueous solution. *Earth Planet. Sci. Lett.* **1984**, *67*, 70–78. [CrossRef]
35. Alderton, D.H.M.; Pearce, J.A.; Potts, P.J. Rare earth element mobility during granite alteration: Evidence from southwest England. *Earth Planet. Sci. Lett.* **1980**, *49*, 149–165. [CrossRef]

36. Dawood, Y.H.; Abd El-Naby, H.H.; Sharafeldin, A.A. Influence of the alteration processes on the origin of uranium and europium anomalies in trachyte, central Eastern Desert, Egypt. *J. Geochem. Explor.* **2004**, *88*, 15–27. [CrossRef]
37. Leybourne, M.I.; Peter, J.M.; Layton-Matthews, D.; Volesky, J.; Boyle, D.R. Mobility and fractionation of rare earth elements during supergene weathering and gossan formation and chemical modification of massive sulfide gossan. *Geochim. Cosmochim. Acta* **2006**, *70*, 1091–1112. [CrossRef]
38. Michard, A. Rare earth element systematics in hydrothermal fluids. *Geochim. Cosmochim. Acta* **1989**, *53*, 745–750. [CrossRef]
39. Kholodov, V.N.; Butuzova, G.Y. Siderite formation and evolution of sedimentary iron ore deposition in the Earth's history. *Geol. Ore Depos.* **2008**, *50*, 299–319. [CrossRef]
40. Skala, G.; Hollabaugh, C.L. Goethite after siderite: The presence of goethite after siderite pseudomorphs in a pegmatic matrix from Lake George, Colorado. *Geol. Soc. Am.* **2012**, *44*, 6.
41. Makkoudi, D. Minéralisations Pb-Ba de M'fiss: Etude Géologique et Contribution à la Gîtologie des Gisements du Tafilalet. Ph.D. Thesis, University Mohammed V, Rabat, Morocco, 1995.
42. Garasic, V.; Jurkovic, I. Geochemical characteristics of different iron ore types from the Southern Tomašica deposit, Ljubija, NW Bosnia. *Geol. Croat.* **2012**, *65*, 255–270. [CrossRef]
43. Markl, G.; von Blanckenburg, F.; Wagner, T. Iron isotope fractionation during hydrothermal ore deposition and alteration. *Geochim. Cosmochim. Acta* **2006**, *70*, 3011–3030. [CrossRef]
44. Torres Ruiz, J. Genesis and evolution of the Marquesado and adjacent ore deposits, Granada, Spain. *Econ. Geol.* **1983**, *78*, 1657–1673. [CrossRef]
45. Decrée, S.; De Putter, T.; Yans, J.; Moussi, B.; Recourt, P.; Jamoussi, F.; Bruyère, D.; Dupuis, C. Iron mineralisation in Mio-Pliocene sediments of the Tamra iron mine (Nefza mining district, Tunisia): Mixed influence of pedogenesis and hydrothermal alteration. *Ore Geol. Rev.* **2008**, *33*, 397–410. [CrossRef]
46. Palinkaš, L.; Damyanov, Z.K.; Borojević Šoštarić, S.; Strmić Palinkaš, S.; Marinova, I. Divergent drift of Adriatic-Dinaridic and Moesian carbonate platforms during the rifting phase witnessed by triassic MVT Pb-Zn and SEDEX deposits; a metallogenic approach. *Geol. Croat.* **2016**, *69*, 75–78. [CrossRef]
47. Brookins, D.G. *Eh-pH Diagrams for Geochemistry*; Springer: Berlin, Heidelberg, 1988; ISBN 3540184856, 0387184856, 9780387184852, 9783540184850.
48. Pracejus, B.; Bolton, B.R.; Frakes, L.A.; Abbott, M. Rare-earth element geochemistry of supergene manganese deposits from Groote Eylandt, Northern Territory, Australia. *Ore Geol. Rev.* **1990**, *5*, 293–314. [CrossRef]
49. Post, J.E. Manganese oxide minerals: Crystal structures and economic and environmental significance. *Proc. Natl. Acad. Sci. USA* **1999**, *96*, 3447–3454. [CrossRef] [PubMed]
50. Bruyère, D.; De Putter, T.; Decrée, S.; Dupuis, C.; Fuchs, Y.; Jamoussi, F.; Perruchot, A.; Arbey, F. Miocene karsts and associated Fe–Zn-rich minerals in Aïn Khamouda (Central Tunisia). *J. Afr. Earth Sci.* **2010**, *57*, 70–78. [CrossRef]
51. Koppi, A.J.; Edis, R.; Field, D.J.; Geering, H.R.; Klessa, D.A.; Cockayne, D.J.H. Rare earth element trends and cerium-uranium-manganese associations in weathered rock from Koongarra, Northern Territory, Australia. *Geochim. Cosmochim. Acta* **1996**, *60*, 1695–1707. [CrossRef]
52. Pagel, M.; Braun, J.; Muller, J. Mécanismes de fractionnement géochimique des terres rares, de l'uranium et du thorium lors des altérations supergènes. In *Séminaire ORSTOM 90: Organisation et Fonctionnement des Altérites et des Sols*; Wackermann, J.M., Ed.; ORSTOM: Bondy, France, 1990; pp. 219–226.
53. De Putter, T.; André, L.; Bernard, A.; Dupuis, C.; Jedwab, J.; Nicaise, D.; Perruchot, A. Trace element (Th, U, Pb, REE) behaviour in a cryptokarstic halloysite and kaolinite deposit from Southern Belgium: Importance of "accessory" mineral formation for radioactive pollutant trapping. *Appl. Geochem.* **2002**, *17*, 1313–1328. [CrossRef]
54. Nicaise, D.; André, L.; Jedwab, J.; Dupuis, C.; De Putter, T. Neoformed LREE phosphates at the nanometer scale, in acid low temperature weathering: Consequences in rare earth elements, uranium and thorium trapping. *C. R. Acad. Sci. Paris* **1996**, *323*, 113–120.
55. Braun, J.J.; Pagel, M.; Muller, J.P.; Bilong, P.; Michard, A.; Guillet, B. Cerium anomalies in lateritic profiles. *Geochim. Cosmochim. Acta* **1990**, *54*, 781–795. [CrossRef]
56. Decrée, S.; Deloule, É.; Ruffet, G.; Dewaele, S.; Mees, F.; Marignac, C.; Yans, J.; De Putter, T. Geodynamic and climate controls in the formation of Mio–Pliocene world-class oxidized cobalt and manganese ores in the Katanga province, DR Congo. *Miner. Depos.* **2010**, *45*, 621–629. [CrossRef]

57. Kamineni, D.C.; Chung, C.F.; Dugal, J.J.B.; Ejeckam, R.B. Distribution of uranium and thorium in core samples from the Underground Research Laboratory lease area, southeastern Manitoba, Canada. *Chem. Geol.* **1986**, *54*, 97–111. [CrossRef]
58. Decrée, S.; Marignac, C.; De Putter, T.; Yans, J.; Clauer, N.; Dermech, M.; Aloui, K.; Baele, J.M. The Oued Belif hematite-rich breccia: A Miocene iron oxide Cu-Au-(U-REE) deposit in the Nefza mining district, Tunisia. *Econ. Geol.* **2013**, *108*, 1425–1457. [CrossRef]
59. Farmer, J.G.; Lovell, M.A. Natural enrichment of arsenic in Loch Lomond sediments. *Geochim. Cosmochim. Acta* **1986**, *50*, 2059–2067. [CrossRef]
60. Bau, M.; Dulski, P. Distribution of yttrium and rare-earth elements in the Penge and Kuruman iron-formations, Transvaal Supergroup, South Africa. *Precambrian Res.* **1996**, *79*, 37–55. [CrossRef]
61. Cotten, J.; Le Dez, A.; Bau, M.; Caroff, M.; Maury, R.C.; Dulski, P.; Fourcade, S.; Bohn, M.; Brousse, R. Origin of anomalous rare-earth element and yttrium enrichments in subaerially exposed basalts: Evidence from French Polynesia. *Chem. Geol.* **1995**, *119*, 115–138. [CrossRef]
62. Castor, S.B.; Hendrick, J.B. Rare Earth Elements. In *Industrial Minerals and Rocks*; Kogel, J.E., Trivedi, N.C., Barker, J.M., Eds.; Society for Mining, Metallurgy and Exploration: Littleton, CO, USA, 2006; pp. 769–792. ISBN 4186530777.
63. Fodor, R.V.; Frey, F.A.; Bauer, G.R.; Clague, D.A. Ages, rare-earth element enrichment, and petrogenesis of tholeiitic and alkalic basalts from Kahoolawe Island, Hawaii. *Contrib. Mineral. Petrol.* **1992**, *110*, 442–462. [CrossRef]
64. Cocker, M.D. Lateritic, supergene rare earth element (REE) deposits. In *48th Annual Forum on the Geology of Industrial Minerals*; Arizona Geological Survey: Scottsdale, AZ, USA, 2012; pp. 1–20.
65. Leybourne, M.I.; Johannesson, K.H. Rare earth elements (REE) and yttrium in stream waters, stream sediments, and Fe-Mn oxyhydroxides: Fractionation, speciation, and controls over REE + Y patterns in the surface environment. *Geochim. Cosmochim. Acta* **2008**, *72*, 5962–5983. [CrossRef]
66. Ayora, C.; Macías, F.; Torres, E.; Nieto, J.M. Rare Earth Elements in Acid Mine Drainage. In *XXXV Reunión de la Sociedad Española de Mineralogía*; Sociedad Espanola de Mineralogia: Huelva, Spain, 2015; pp. 1–22.
67. Coppin, F.; Berger, G.; Bauer, A.; Castet, S.; Loubet, M. Sorption of lanthanides on smectite and kaolinite. *Chem. Geol.* **2002**, *182*, 57–68. [CrossRef]
68. Banfield, J.F. Apatite Replacement and Rare Earth Mobilization, Fractionation, and Fixation During Weathering. *Clays Clay Miner.* **1989**, *37*, 113–127. [CrossRef]
69. Hannigan, R.E.; Sholkovitz, E.R. The development of middle rare earth element enrichments in freshwaters: Weathering of phosphate minerals. *Chem. Geol.* **2001**, *175*, 495–508. [CrossRef]
70. Köhler, S.J.; Harouiya, N.; Chaïrat, C.; Oelkers, E.H. Experimental studies of REE fractionation during water–mineral interactions: REE release rates during apatite dissolution from pH 2.8 to 9.2. *Chem. Geol.* **2005**, *222*, 168–182. [CrossRef]
71. Göb, S.; Wenzel, T.; Bau, M.; Jacob, D.E.; Loges, A.; Markl, G. The redistribution of rare-earth elements in secondary minerals of hydrothermal veins, Schwarzwald, Southwestern Germany. *Can. Mineral.* **2011**, *49*, 1305–1333. [CrossRef]
72. Lottermoser, B.G. Rare-earth element mineralisation within the Mt. Weld carbonatite laterite, Western Australia. *Lithos* **1990**, *24*, 151–167. [CrossRef]
73. De Putter, T.; Charlet, J.-M.M.; Quinif, Y. REE, Y and U concentration at the fluid-iron oxide interface in late cenozoic cryptodolines from Southern Belgium. *Chem. Geol.* **1999**, *153*, 139–150. [CrossRef]
74. Bouabdellah, M.; Margoum, D. Geology, Fluid Inclusions, and Geochemistry of the Aouli Sulphide-Fluorite-Barite Vein Deposit (Upper Moulouya District, Morocco) and Its Relationships to Pangean Rifting and Opening of the Tethys and Central Atlantic Oceans. In *Mineral Deposits of North Africa, Mineral Resource Reviews*; Bouabdellah, M., Slack, J.F., Eds.; Springer: Cham, Switzerland, 2016; pp. 291–305.
75. Bouabdellah, M.; Zemri, O.; Jébrak, M.; Klügel, A.; Levresse, G.; Maacha, L.; Gaouzi, A.; Souiah, M. Geology and Mineralogy of the El Hammam REE-Rich Fluorite Deposit (Central Morocco): A Product of Transtensional Pangean Rifting and Central Atlantic Opening. In *Mineral Deposits of North Africa, Mineral Resource Reviews*; Bouabdellah, M., Slack, J.F., Eds.; Springer: Cham, Switzerland, 2016; pp. 307–324.

76. Cheilletz, A.; Gasquet, D.; Filali, F.; Archibald, D.A.; Nespolo, M. A Late Triassic 40Ar/39Ar age for the El Hammam high-REE fluorite deposit (Morocco): Mineralization related to the Central Atlantic Magmatic Province. *Miner. Depos.* **2010**, *45*, 323–329. [CrossRef]
77. Margoum, D.; Bouabdellah, M.; Klügel, A.; Banks, D.A.; Castorina, F.; Cuney, M.; Jébrak, M.; Bozkaya, G. Pangea rifting and onward pre-Central Atlantic opening as the main ore-forming processes for the genesis of the Aouli REE-rich fluorite–barite vein system, upper Moulouya district, Morocco. *J. Afr. Earth Sci.* **2015**, *108*, 22–39. [CrossRef]